

Abstract

Perkey, David Wayne. Long-term sediment accumulation rates and organic carbon burial on the middle Eel shelf: northern California. (Under the direction of Elana L. Leithold and Neal E. Blair)

The Earth's continental margins are currently the primary site of organic carbon burial. Over geologic time the burial and preservation of organic carbon plays a significant role in regulating atmospheric composition. The efficiency at which organic carbon is buried is influenced by many factors that include dissolved oxygen levels, sedimentation rates, and organic carbon composition. The Eel River shelf off of northern California is a well-studied system that is ideal for exploring the interplay between some of these factors

Examination of a recent piston core taken from the middle Eel shelf off the coast of northern California revealed that sediment accumulation rates over the last five decades are elevated when compared to the previous 1900 years. ^{14}C -dating of woody debris and clay organic carbon indicate that accumulation rates range between 0.9-1.4 cm/yr over the later half of the 20th century. However, prior to 1964-1955 sediment accumulation rates were 0.15 ± 0.02 cm/yr. A change in core stratigraphy was also observed at a depth corresponding to the middle 20th century. Modern shelf sediments were finer grained and dominated by more frequent flood deposits when compared to sediments deposited before the later half of the past century. Despite the recent increase in preserved flood layers off shore of the Eel River, correlation between reconstructed river discharge of the

nearby Sacramento River and the Eel River revealed that current levels of discharge are not unique over the past 2000 years. Therefore increased precipitation is not thought to be the key factor for the change in sedimentation on the middle shelf. Instead, the peak of logging activity in the basin was correlated to change in sedimentation. ^{14}C -ages of woody debris recovered from the piston core revealed that old growth wood was present only in shelf sediments below a depth that corresponds to the 1955-1964 era. Therefore land use alteration is a key reason for the change in sediment accumulation rates on the middle Eel shelf.

The 6-11 fold increase in modern sediment accumulation rates was linked to changes in the content of organic carbon being buried on the shelf. Unlike other studies, the majority of the organic carbon being buried on the Eel shelf was found within the coarse ($>25\mu\text{m}$) fraction. Modern mean %OC of this fraction was twice the mean %OC prior to 1955-1964. Analysis of the sedimentary organic carbon associated with clay particles revealed organic carbon loading (OC/SA) to be 30% higher when accumulation rates were lower. An isotopic mass balance of the organic carbon sources loaded on the clays showed that approximately half (40-60%) of the OC was from a kerogen source. This is true for samples deposited before and after the change in sedimentation rates. Furthermore, the increase in %OC associated with lower sedimentation rates is due to higher amounts of marine and terrestrial OC being preserved on the clay particles in response to longer residence times in both the regolith and benthic mixed layer.

**LONG-TERM SEDIMENT ACCUMULATION RATES AND ORGANIC
CARBON BURIAL ON THE MIDDLE EEL SHELF: NORTHERN CALIFORNIA**

by

David Wayne Perkey

A thesis submitted to the graduate faculty of
North Carolina State University
in partial fulfillment of the
requirements for the Degree of
Master of Science

MARINE, EARTH AND ATMOSPHERIC SCIENCES:

EARTH SCIENCE

Raleigh

2003

APPROVED BY:

Co-chair of Advisory Committee

Co-chair of Advisory Committee

Dedication

This thesis is dedicated in loving memory of my grandparents:

Doris Montminy and Charles and Ruth Perkey.

Autobiography

I was born to Arlyn and Cecile Perkey on October 12, 1976 in Bedford, Indiana. While I was a young child our family moved around a lot, and it was during our few years spent in southeastern Maine that I developed a love for the ocean. We departed Maine in 1983 and put down roots in Morgantown, West Virginia, where I was raised. Despite growing up in a land-locked, mountainous state, I always maintained my fascination with the sea.

In 1995 I left Morgantown for Columbia, SC to attend the University of South Carolina as a marine science major. While attending USC, I began working in a marine organic-geochemistry lab under the guidance of Dr. Miguel Goni. After graduation from USC in 1999 with my B.S., I decided to matriculate to North Carolina State University to further my education in the realm of marine sediments. Now, in 2003, my formal education is completed at long last. Where the winding road of life will take me from here is anyone's guess, but I plan on enjoying the view along the way.

Acknowledgements

My work on this project would not have been started without the guidance of Dr. Miguel Goni and Maria Teixeira-Votava. Their support, friendship, and teachings are largely responsible for why I'm where I'm at today.

I want to thank Dave Bernstein and Lauren Caslin for being my partners in crime when I first arrived at N.C. State. Along that same note, I also need to thank my "Lake Park Roomies": Chas, Jana and Jason. I also want to thank Jennifer Holmes, Shawn Ford, Kelly Peeler and Samantha Rider for all their assistance in processing my cores. I would probably still be slicing piston core sections without your help. Further thanks must go to Jennifer Holmes for all her helpful thoughts and willingness to share ideas. I'd like to thank Katie Holman for all the coffee breaks and lunches we took during the writing stages of this work. Nothing is more important than some social interaction and caffeine when you've been staring blankly at a computer screen for countless hours.

I must thank my committee members: Dr. Lonnie Leithold, Dr. Neal Blair and Dr. Dave DeMaster for their time, resources, knowledge, and critique of this work. In particular I would like to thank Lonnie and Neal for their patience and dedication to me as a student. You make good shepherds.

Lastly, of course, I must thank my parents, Arlyn, Cecile, Dan, Marial, Roger and Shirley, my brothers, Jim, Shaun and Jack, my sisters, Karen, Anna, Kathy and Kelli, and my grandfather, Leo. Though not all of you are family by blood, you are all family by heart, and without your love and support I could not have made it to this point in my life.

Table of Contents

	Page
LIST OF FIGURES_____	vi
LIST OF TABLES_____	ix
INTRODUCTION_____	1
METHODS_____	8
RESULTS_____	14
DISCUSSION_____	40
SUMMARY AND CONCLUSIONS_____	62
REFERENCES_____	64
APPENDICIES_____	74
Grain size data for cores_____	75
Organic carbon data for cores_____	77
14-Carbon data for cores_____	79

List of Figures

	Page
Figure 1.1	Eel River Watershed_____ 4
Figure 3.1	(a) Density log of K70 box core_____ 15
	(b) Density log of K70 piston core_____ 15
Figure 3.2	(a) Plot of depth vs. ^{14}C age of wood_____ 17
	(b) Plot of dry bulk density vs. ^{14}C age of wood_____ 17
Figure 3.3	(a) Plot of depth vs. ^{14}C age of clay_____ 19
	(b) Plot of dry bulk density vs. ^{14}C age of clay_____ 19
Figure 3.4	(a) Background accumulation rate based wood ^{14}C ages____ 21
	(b) Background accumulation rate based on clay ^{14}C ages____ 21
Figure 3.5	Pie charts of weight % distribution of clay_____ 24
Figure 3.6	(a) Piston core flood layers identified by density_____ 25
	(b) Piston core flood layers identified by grain-size_____ 25
Figure 3.7	Box and Piston core flood layer comparison_____ 27
Figure 3.8	(a) Plot of depth vs. weight % OC for all size fractions____ 28
	(b) Plot of depth vs. atomic C/N for all size fractions____ 28
	(c) Plot of depth vs. $\delta^{13}\text{C}$ for all size fractions_____ 28
Figure 3.9	Depth vs. weight % OC and OC/SA_____ 32
Figure 3.10	Depth vs. weight % clay and clay $\delta^{13}\text{C}$ _____ 33
Figure 3.11	Depth vs. clay surface area_____ 34
Figure 3.12	XRD diffractograms of K-saturated, air-dried_____ 37

List of Figures (continued)

	Page
Figure 3.13	(a) XRD diffractograms of K-saturated, 350°C _____ 38
	(b) XRD diffractograms of K-saturated, 550°C _____ 38
Figure 3.14	(a) XRD diffractograms of Mg-saturated, air-dried _____ 39
	(b) XRD diffractograms of Mg-saturated, ethylene glycol _____ 39
Figure 4.1	Age estimation of box core flood layers _____ 42
Figure 4.2	Age estimation of piston core flood layers _____ 44
Figure 4.3	(a) Eel and Sacramento River mean annual discharges _____ 45
	(b) Eel and Sacramento River 6-year mean discharges _____ 45
Figure 4.4	Reconstructed discharge of the Sacramento River _____ 47
Figure 4.5	Depth vs. clay OC/SA _____ 53
Figure 4.6	(a) Clay surface area vs. OC/SA _____ 54
	(b) Clay weight %OC vs. OC/SA _____ 54
Figure 4.7	Distribution of kerogen, terrestrial and marine OC on shallow samples
	(a) Fractional composition of TOC _____ 59
	(b) Fractional composition of TOC normalized to SA _____ 59
	(c) Fractional composition of TOC normalized to weight %OC _____ 59

List of Figures (continued)

	Page
Figure 4.8	
Distribution of kerogen, terrestrial and marine OC on deep samples	
(a) Fractional composition of TOC _____	60
(b) Fractional composition of TOC normalized to SA _____	60
(c) Fractional composition of TOC normalized to weight %OC _____	60

List of Tables

	Page
Table 3.1	Detailed grain-size analysis_____23
Table 3.2	Budget & distribution of weight %OC_____30

1. Introduction

Continental margins are the primary site for accumulation of sediments (Erickson, 1996; Seibold and Berger, 1996). In association with sediment, organic carbon is also buried and preserved. Even though less than 1% of the total terrestrial organic carbon delivered to the oceans is buried within marine sediments, continental margins are currently the primary site for organic carbon burial, and therefore play a significant role in regulating atmospheric compositions of carbon dioxide and oxygen on geologic time scales (Berner, 1982, 1989; Hedges and Keil, 1995).

Factors that could influence the rate of organic carbon burial are numerous and include dissolved oxygen levels, sedimentation rates, mineral particle association, and organic carbon composition (Hedges and Keil, 1995; Hartnett et al., 1998). Because oxygen is required to support an active benthos, and is the most relevant oxidant in the series of electron acceptors in remineralization of organic carbon, the residence time of particles in an oxic environment has been strongly correlated to organic carbon burial efficiency (Hartnett et al., 1998). In turn, accumulation rates are thought to affect the preservation of organic carbon due to the fact that bacterial and animal activities are generally highest at the sediment surface, where oxygen levels are also highest (Hedges and Keil, 1995). Rapid deposition rates remove organics from this active zone of destruction quickly, which generally increases organic carbon preservation. Other investigations have concluded that organic carbon is preserved due to its association with mineral particles, where it may be protected in intra- or inter-

granular pores (Bock and Mayer, 2000). A direct correlation between mineral surface area and organic carbon concentrations supports the idea that fine, clay-sized mineral particles play a role in the burial and preservation of organic carbon (Mayer, 1994a, b; Keil et al., 1994; Ransom et al., 1998). While the depositional environment likely influences organic preservation, the type of organic matter buried may also be a factor. Sedimentary organic matter may include fractions of different ages, reactivity, and preservation potential (Blair et al., 2003).

The Eel River shelf off the coast of northern California is a well-studied area and is an ideal location to explore the interplay of some of the factors that control organic carbon preservation. Sediment accumulation rates on the shelf have been shown to be high, but variable over several different time scales (Creamer, 1998; Sommerfield and Nittrouer, 1999; Sommerfield et al., 2002). In addition to rapid accumulation rates, mid-shelf sediments are predominately fine-grained and therefore have high surface areas. Previous work has shown that the organic carbon associated with these mineral particles include fractions of different ages and reactivities that range from modern marine and terrestrial carbon to ancient (kerogen) carbon (Leithold and Blair, 2001; Blair et al., 2003). In this study a detailed, long-term record of the upper 3 meters of the seabed on the middle Eel shelf was examined to ascertain how the changes in sediment supply from land and accumulation rates offshore have controlled carbon burial on annual to millennial time scales.

The Eel River Watershed

The Eel River drains a small (approx. 8,000 km²), mountainous, tectonically active basin in northern California (Fig. 1.1; Milliman and Syvitski, 1992). Primarily sedimentary rocks of the Jurassic-Tertiary Franciscan Complex, including coherent sandstone blocks and sheared, shale-rich *mélange*, underlie the basin. Sandstones typically underlie areas dominated by forest cover, while grassland regions of the basin are underlain by shaley *mélange* material (Kelsey, 1980; Blake et al., 1988). Maximum rates of tectonic uplift throughout the basin range between 1-5 mm/yr due to the subduction of the Gorda Plate beneath the North American Plate (Clarke, 1992; Orange, 1999; Burger et al., 2001).

The Eel Basin is strongly affected by winter storms. Annual rainfall ranges between 125-250 centimeters (Kelsey, 1980), with 80% of that precipitation falling during the winter months (Syvitski and Morehead, 1999). As a result, over 90% of the river's runoff occurs in the months from November to May (Sommerfield and Nittrouer, 1999). Approximately 50% of the annual sediment load transported by the Eel River is discharged in 1-2 week periods associated with floods from winter storms (Brown and Ritter, 1971). Much of this sediment transported by the river is derived from mass-wasting events. A study of the Van Duzen River suggested that earthflows along the riverbanks and grass covered *mélange* areas, along with debris slides from the more consolidated sandstone slopes, provide a major sediment source to the river (Kelsey, 1980).

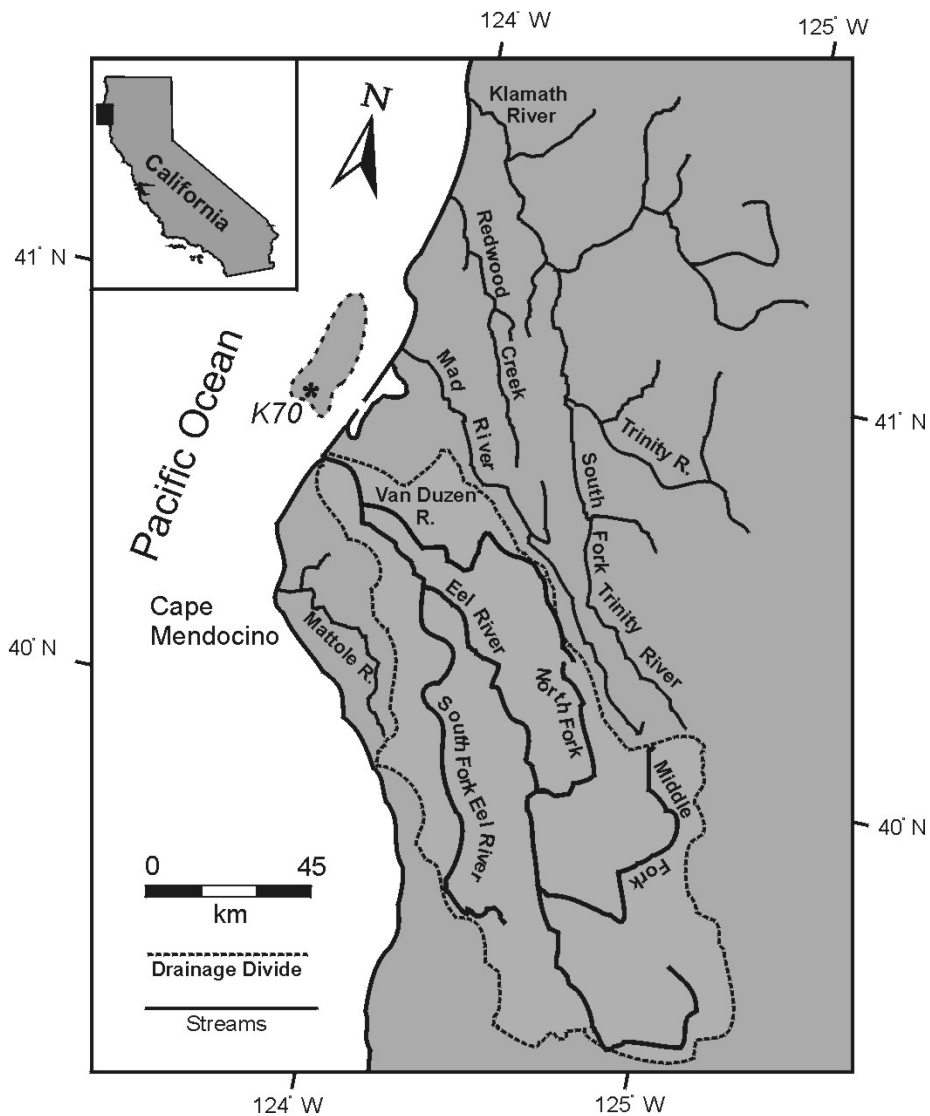


Figure 1.1. Location of the Eel River watershed and shelf in northern California. Sample station K70 is indicated with the dot on the Eel shelf. A recently mapped flood deposit (1997) is also indicated with shading north of the Eel mouth.

Land use in the basin has varied over time and location. Aboriginal tribes inhabited the area for thousands of years and periodically used fire as a form of vegetation management (U.S. Environmental Protection Agency, 1999a, b). The first Euro-American colonization did not take place until the mid 1800's. Most of these early settlers were ranchers, and primarily used the land for farming and grazing (U.S. Environmental Protection Agency, 1999a, b). Timber industry developed in parts of the basin soon after Euro-American colonization, however, due to the remoteness and steep terrain of the basin much of the timber was inaccessible for harvest. After World War II modern equipment allowed for the harvesting of much of the remaining timber stands. Timber production in the area reached its peak in the late 1950's, but still remains a significant land use today (Hackett, 1999; U.S. Environmental Protection Agency, 1999a, b). Current significant land uses also include agricultural grazing, recreation, and residential development.

The combination of tectonic activity, weak sedimentary rocks, and wet winter conditions results in a system with high sediment yield (Milliman, 1997). Studies also indicate that anthropogenic alterations of land use by grazing, logging, and road building often increases erosion (Goff, 1997; Milliman, 1997; Rooney and Smith, 1999; VanGreen et al., 1999; Hilfinger et. al, 2001). The Eel River has the highest sediment yield (i.e., sediment eroded per unit drainage area) in the contiguous United States ($1700 \text{ t/km}^2/\text{yr}$), despite the fact that the river is only discharging sediment for half of the year (Brown and Ritter, 1971; Milliman

and Syvitski, 1992). Such a large discharge of sediment provides for rapid accumulation rates on the continental shelf.

Eel Shelf Environment

The Eel shelf runs from Cape Mendocino to Trinidad Head, and extends out to the 150 m isobath, making the shelf approximately 10-20 km wide (Sommerfield and Nittrouer, 1999). An across-shelf gradation from nearshore sandy deposits to offshore muddy deposits exists, with a narrow transition zone found between the 50-60 m isobaths (Leithold, 1989). The Eel River is the largest source of fine-grained sediment to the northern California coast (15×10^6 metric tons/yr), most of which is delivered during storm events (Sommerfield et al., 2001).

The dominant current systems on the shelf vary seasonally. The equatorially flowing California Current is strongest during the summer months, however, during the winter months this current weakens and the north flowing, inshore Davidson Current assumes dominance (Strub and Corinne, 2002). However, transport of winter flood plumes is typically dominated by strong, storm induced winds out of the south. This results in flood sediments being transported north of the river mouth (Geyer et al., 2000).

Specific mapping of a flood event in 1995 illustrated that flood related deposition was centered approximately 30 kilometers north of the river mouth around the 70 m isobath (Wheatcroft and Borgeld, 2000). It is estimated that 20-25% of the annual fluvial suspended load is trapped on the shelf (Sommerfield

and Nittrouer, 1999; Wheatcroft and Borgeld, 2000). The rest is either transported off the shelf and down slope, or is stored in the near-shore sandy deposits (Sommerfield and Nittrouer, 1999). Holocene mud deposits dominate the shelf, as a result of the deposition of riverine sediments. Examination of the small-scale stratigraphy of shelf sediments revealed that clay rich flood layer deposits were preserved and play a large role in sediment accumulation rates (Leithold, 1989; Sommerfield and Nittrouer, 1999).

A study by Sommerfield and Nittrouer (1999) utilized ^{210}Pb activities and found that modern accumulation rates on the middle shelf ranged between 0.5-0.8 cm/yr. ^{137}Cs activities from that study indicated that accumulation rates appeared to increase after 1954. A later study (Sommerfield et al., 2002) measured ^{14}C activities and reported that from A.D. 405-495 to ca. 1954 accumulation rates for the mid-shelf ranged from 0.02-0.18 cm/yr. Again ^{137}Cs activities revealed a sudden increase in sedimentation ca. 1954 (0.3 cm/yr) when compared to the ^{14}C based accumulation rate. These studies offer solid evidence that accumulation rates over the last 50 years have been faster than the previous 50 years and beyond. This recent increase in accumulation has been attributed to the increase in flood frequency of the Eel River over this time frame (Creamer, 1998; Sommerfield et al., 2002).

Studies conducted on the Eel shelf have also investigated organic matter associated with recent shelf deposits. Modern shelf clays have been found to contain 1-2% organic carbon by weight (Leithold and Blair, 2001). Characterization of this carbon revealed that mid-shelf sediments had a fairly

constant $\delta^{13}\text{C}_{\text{PDB}}$ value of $-24.4\pm 0.3\%$. Though deposition has been recent, newly deposited sediments on the shelf have been shown to have a significant proportion of ancient (kerogen) carbon associated with them (Leithold and Blair, 2001; Blair et al., 2003). When the $\delta^{13}\text{C}_{\text{PDB}}$ values of modern marine sediments were compared to those of mélange bedrock samples from the Eel River watershed, a near identical $\delta^{13}\text{C}_{\text{PDB}}$ value of $-24.3\pm 0.6\%$ was found (Leithold and Blair, 2001). This similarity suggested that a large component of organic carbon found on the Eel Shelf was derived from the Franciscan mélange complex of the Eel watershed. A carbon isotope budget on these clay sediments (Blair et al., 2003) revealed that nearly half of the organic carbon associated with the clay particles was in fact ancient, kerogen carbon. The age of such carbon indicates that it has survived significant biogeochemical processing during its formation and is now nonreactive (Blair et al., 2003). Such old, recalcitrant carbon would most likely escape oxidation in the benthic mixed zone and be preserved in the geologic record.

2. Methods

Core Collection and Processing

Marine sediments were obtained from station K70 (Fig. 1.1) using piston and box corers deployed from the *R.V. Thomas Thompson* in August of 1999 at 70 meters water depth, approximately 11 kilometers north of the Eel River mouth. The box core was approximately 40 centimeters in length, and was subcored with plastic core liners using a piston apparatus. The piston core taken at this site

measured approximately 3.5 meters in total length. Both piston and box cores were scanned with a GEOTEK Multi-Sensor Core Logger to provide density and magnetic susceptibility profiles of the cores. The cores were then placed in frozen storage on the ship until shipment to NCSU. All core sections were shipped in coolers with dry ice and placed in freezers upon arrival. Before dissection the cores were partially thawed at room temperature and a description was made to record any visible layers or breaks in the core. All core sections were dissected at 1 cm intervals, placed in glass jars or plastic bags, and returned to the freezer. Due to contact with the wooden core extruder, the bottom centimeter of every core section was discarded.

Sample Separation & Grain Size Analysis

Samples from approximately every 10 centimeters in the piston core and every 2 centimeters in the box core were selected for separation into size fractions. The clay ($<4 \mu\text{m}$), medium-fine silt ($4\text{-}25 \mu\text{m}$), and coarse silt and sand ($>25 \mu\text{m}$) size fractions were isolated as follows. Samples were homogenized with a glass or metal stir rod and approximately 5 to 15 grams of bulk sample were washed through a $25 \mu\text{m}$ stainless steel sieve with deionized water. Material greater than $25 \mu\text{m}$ was removed from the sieve and frozen. Material that passed through the sieve was further fractionated into $<25 \mu\text{m}$ and $<4 \mu\text{m}$ sizes through standard settling techniques that utilize Stokes Law (Blatt et al.1980). This fractionation was done with deionized water through either the use of pipette methods or a peristaltic pump. After addition of dispersant (sodium

metaphosphate 1 g/L) to prevent flocculation, the volume of solution in the cylinder was recorded. The solution was then mixed thoroughly with a metal or glass stir rod for at least 1 minute. After mixing, the $<25\ \mu\text{m}$ fraction was collected by withdrawing 40 ml of solution out of the cylinder from a random depth with a pipette. Recovery of the $<4\ \mu\text{m}$ fraction was then started by recording the new volume of the cylinder. Glass tubing was placed 10 cm below the water line and clamped into place. MasterFlex size 25 viton tubing was used to connect the glass tube to a peristaltic pump. The contents of the cylinder were thoroughly remixed with a glass or metal stir rod, covered, and allowed to settle for two hours (time determined by Stokes Law). At the end of two hours all contents above the 10 cm mark were pumped into a 1000 ml beaker at a rate of 60 ml/min. The ending volume of the cylinder was recorded, and the solution in the beaker was placed in glass centrifuge tubes. The cylinder was then refilled to the starting volume with distilled water and the procedure was repeated. Both the $<25\ \mu\text{m}$ and $<4\ \mu\text{m}$ fractions were collected by centrifugation and then dried in vacuo at room temperature. Upon drying, weight percents of each size fraction were calculated and corrected for the dispersant that was added.

To determine experimental error on separation procedures, replicate grain size analyses were run on sediments from a nearby location on the Eel shelf (S100). Measured weight percents of coarse material ($>25\ \mu\text{m}$), medium silt ($4-25\ \mu\text{m}$), and clay ($<4\ \mu\text{m}$) fractions had experimental errors of $\pm 0.75\%$, $\pm 1.3\%$, and $\pm 1.3\%$ respectively ($n=4$).

Samples that were selected for a more detailed grain size analysis were pre-treated with 30 ml of 30% hydrogen peroxide to remove organic matter. After oxidation, the samples were sonicated for two minutes. Wet sieving was then performed to isolate the sand size fraction ($>63 \mu\text{m}$ or 4ϕ). The sand fraction was further fractionated through dry sieving at 0.5ϕ intervals. The fine fraction was separated using the same standard settling techniques mentioned above. Fine material was collected at 0.5ϕ intervals down to 8ϕ ($4 \mu\text{m}$), and then collected at 1.0ϕ intervals down to 12ϕ ($.02 \mu\text{m}$).

Elemental Analysis

All size fractions of sediment that were to be analyzed for organic carbon (OC) and total nitrogen content were first acidified with HCl vapor overnight to remove carbonates. The sediment was then dried in vacuo at room temperature and loaded into tin boats to be analyzed with a Carlo Erba 1108 CHNS analyzer. The OC and N contents were then corrected to account for the weight of dispersant and salt.

$^{13}\text{C}/^{12}\text{C}$ Measurements

The CO_2 gas generated from the organic matter combustion in the CHNS analyzer was collected cryogenically (Blair and Carter, 1992) and analyzed for carbon isotopic ratios using a modified Finnigan MAT Delta E Mass Spectrometer (Hayes et al., 1977). The ratio of $^{13}\text{C}/^{12}\text{C}$ in a sample is reported

relative to that of the PDB standard (Keith and Weber, 1964), utilizing the $\delta^{13}\text{C}$ notation, where

$$\delta^{13}\text{C} = \left[\frac{\left(\frac{^{13}\text{C}}{^{12}\text{C}} \right)_{\text{sample}}}{\left(\frac{^{13}\text{C}}{^{12}\text{C}} \right)_{\text{PDB}}} - 1 \right] \times 1000.$$

$^{14}\text{C}/^{12}\text{C}$ Measurements

Approximately 5 to 15 grams of bulk sample was suspended in deionized water and sonicated for two minutes to help remove any mineral particles from discrete plant fragments. The samples were then separated into $<4 \mu\text{m}$, and $>25 \mu\text{m}$ fractions as previously described in sample separation procedures. Under a microscope, small pieces of discrete wood and plant material were selected from the $>25 \mu\text{m}$ fraction. These pieces of plant material, along with their corresponding clay size fractions were processed separately on the Carlo Erba 1108 CHNS Analyzer. CO_2 gas was collected cryogenically, sent to the WHOI Ocean Sciences AMS facility, and converted to graphite. ^{14}C -analyses were then made by accelerator mass spectrometry. Correction for natural fractionation was accomplished by normalizing the $\delta^{13}\text{C}$ values of the samples to -25‰ . ^{14}C -contents were reported as fraction modern relative to the NBS Oxalic Acid standard (Olsson, 1970).

Surface Area

Approximately 0.3 g of clay material were weighed and rinsed three times with DI water to remove any dispersant. The clay fraction was then freeze-dried and combusted overnight at 350°C to remove the bulk of the organic material. After combustion, samples were degassed at 150°C for 45 minutes and measured for surface area by nitrogen sorption using the multipoint BET method (Branauer et al., 1938) on a Coulter SA 3100 surface area analyzer.

Clay Mineralogy

Samples from various depths in the cores were selected for examination of clay mineral composition. To fully examine the clay mineralogy of sediments, it is a common practice to saturate the clay with different cations (Moore and Reynolds, 1989). In this study each sample went through two different saturation treatments, one with magnesium and the other with potassium. Standard procedures for cation saturation treatments were taken from Dixon and White (1995). After saturation was completed, 5-10 ml of deionized water were added to the clay and mixed to slurry. The slurries were then transferred onto glass slides with a pipette and allowed to air dry under watch glasses. All slides were analyzed on a Rigaku D/Max B automated x-ray diffractometer equipped with a goniometer with a crystal monochromator. Diffraction patterns were recorded by step scanning from 3°-35° 2 θ , with a step size of 0.05 at 2°/min. After an initial scan through the diffractometer, the magnesium-saturated slides were exposed to ethylene glycol vapors in a sealed desiccator for a period of 12 hours, and rerun to

test for the presence of expandable clays (smectite). All slides were run within 1 hour of being removed from the ethylene glycol environment. After an initial scan, the potassium-saturated slides were then heated for six hours at 300°C and rerun on the XRD. These same slides were then reheated to 550°C for another six hours and once again run on the XRD. These heating treatments cause d-space collapsing of certain clays and were used to test for the presence of smectite, chlorite, and kaolinite.

Statistical Analysis

An approximate t-test conducted at the 5% significance level ($\alpha=.05$; Rao, 1998) was utilized to compare the mean values of surface area, weight %OC, organic carbon loading, atomic C/N, $\delta^{13}\text{C}_{\text{PDB}}$, and weight %<25 μm for sediments deposited above 60 cm depth in the core to those sediments deposited below that level.

3. Results

Core Texture

Both cores recovered from K70 had a brown to olive green coloration, and an overall consistency of stiff mud. Pieces of shell and wood debris were disseminated throughout both cores. No fine-scale stratigraphy was apparent upon visual examination. In both the box core and piston core the top 5 cm of sediment was more fluid than sediment encountered below.

The presence of some lower density layers was detected in gamma ray density profiles of the cores (Fig. 3.1). Ten lower density layers were

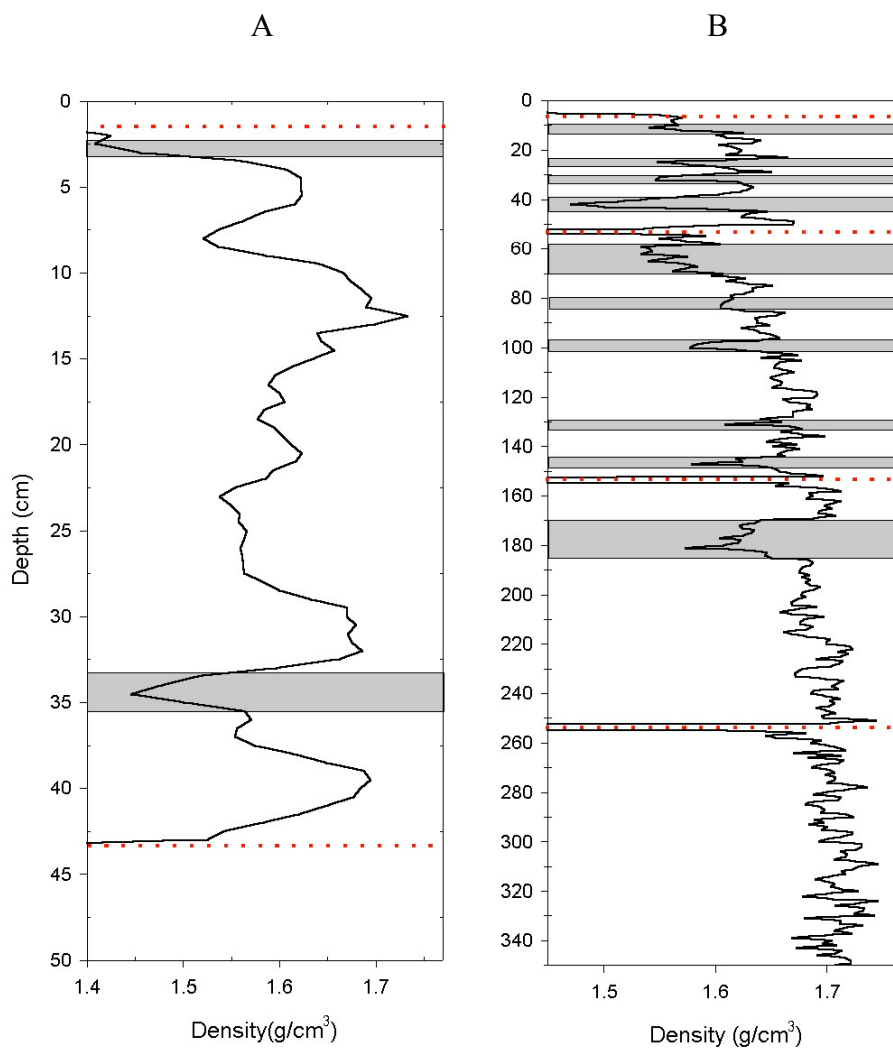


Figure 3.1. Gamma ray density profiles of the box core (A) and piston core (B) from K70. Lower density layers are marked with shaded boxes. Low density returns marked with red dotted lines indicate where the piston core was segmented on ship or the ends of the box core.

encountered in the piston core, and two layers were found in the box core. The distribution of the lower density layers was uneven in the piston core. Half of the lower density layers were found in the upper 70 centimeters, and no distinct layers were seen below a depth of 180 cm (Fig. 3.1). There was a gradual trend from lower to higher density in the piston core, likely reflecting the effects of compaction and dewatering during burial.

Accumulation Rates

Sediment accumulation rates at K70 were calculated using apparent ^{14}C -ages for clay-sized particles and from woody fragments picked from the coarse fraction. Based upon Kelsey (1980), it was hypothesized that large flood events could significantly increase the input of sedimentary carbon from debris slides, and thus deliver sediment with a different organic carbon composition than smaller annual floods. For this reason, samples with high clay content, interpreted to have been deposited during decadal-scale floods, were deliberately not used for ^{14}C analysis. Figure 3.2 shows the apparent ^{14}C age results for the woody fraction. Below 70 centimeters depth, the apparent accumulation rate was 0.17 cm/yr ($r^2=0.96$). The calculated mass flux, which corrects for porosity variations down-core by plotting ^{14}C age versus the sum dry bulk density of sediment (ρ/cm^2), was 0.11 g/cm²/yr ($r^2=0.97$). Wood samples above 46 cm were found to have post-modern ages, and therefore were excluded from both of the regressions.

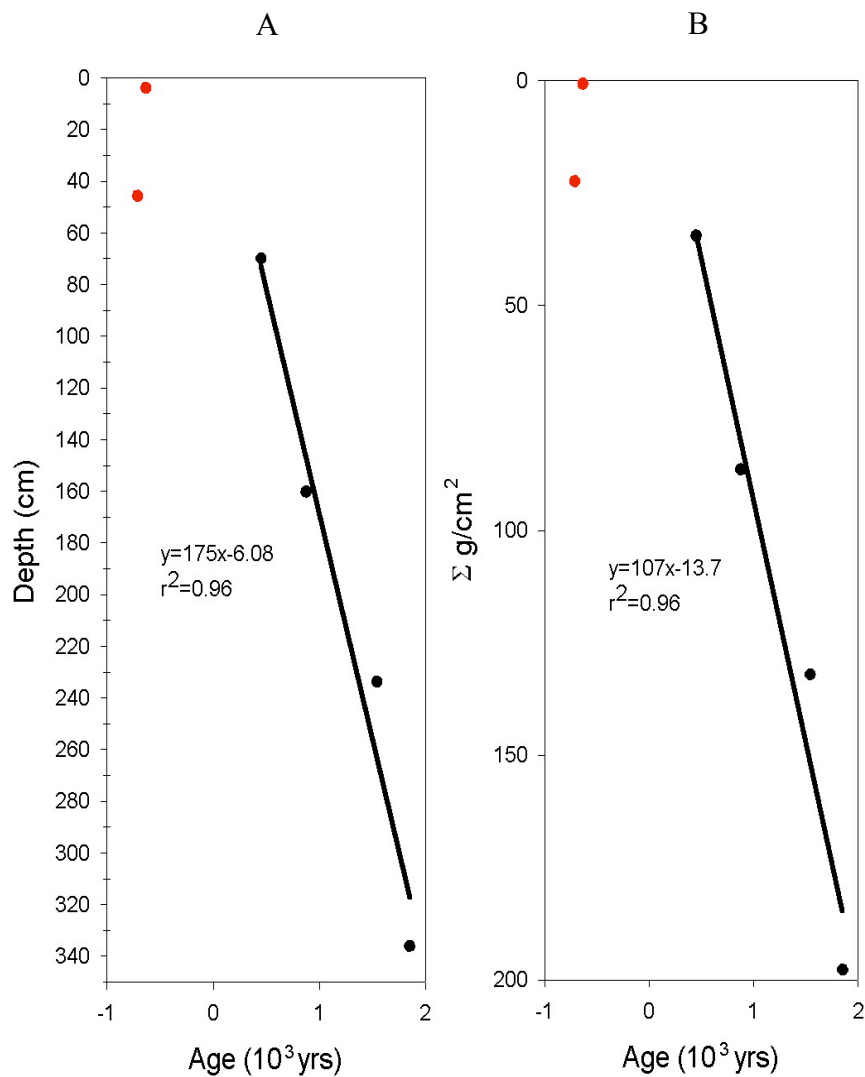


Figure 3.2. ^{14}C ages of woody fibers from the piston core plotted with respect to depth (A) and Σ g/cm² (B). A linear relationship was found in both graphs that indicated accumulation rates of 0.17 cm/yr and 0.11 g/cm²/yr. Red dots indicate samples that had a post-modern age due to enrichment with bomb carbon and were not considered in the least square regression fit.

A very similar accumulation rate was calculated using the clay fraction over the same depth at K70 (Fig. 3.3). Here the sediment accumulation rate was found to be 0.14 cm/yr, and the mass flux was 0.089 g/cm²/yr ($r^2=0.98$; Fig. 3.3). As for the wood fragments, the surface sample was omitted from the regressions due to its exposure to bomb carbon. The sample from 234 cm was also omitted from the regressions because it was suspected to be associated with a flood layer (Fig. 3.3). This issue will be discussed in greater detail later. The resulting accumulation rates of the wood and clay fractions were averaged to obtain an accumulation rate of 0.16 ± 0.02 cm/yr for the region of the piston core below 70 cm.

An approximate accumulation rate for the upper 70 cm of the piston core was also calculated through the use of ¹⁴C data. The futuristic age of the wood fragments at and above 46 cm results from the inclusion of bomb carbon, and thus indicates that the onset of atmospheric weapons testing is recorded at a depth between 46-70 cm in the core. By dating this section of the core to a period of time between 1950-1960 an estimate of a constant accumulation rate of 0.96-1.8 cm/yr was calculated. A previous study by Creamer (1998) found similar results (1.1-1.9 cm/yr) over the same time period in a kasten core taken at K70 in 1995. While this increase in modern accumulation rate is large, a study by Sommerfield et al. (2002) also showed that ¹⁴C based accumulation rates at K70 increased from 0.2-1.8 cm/yr prior to 1954 to 3.0 cm/yr after 1954. This approximate 2-15 fold increase in accumulation brackets the 6-11 fold increase found in this study.

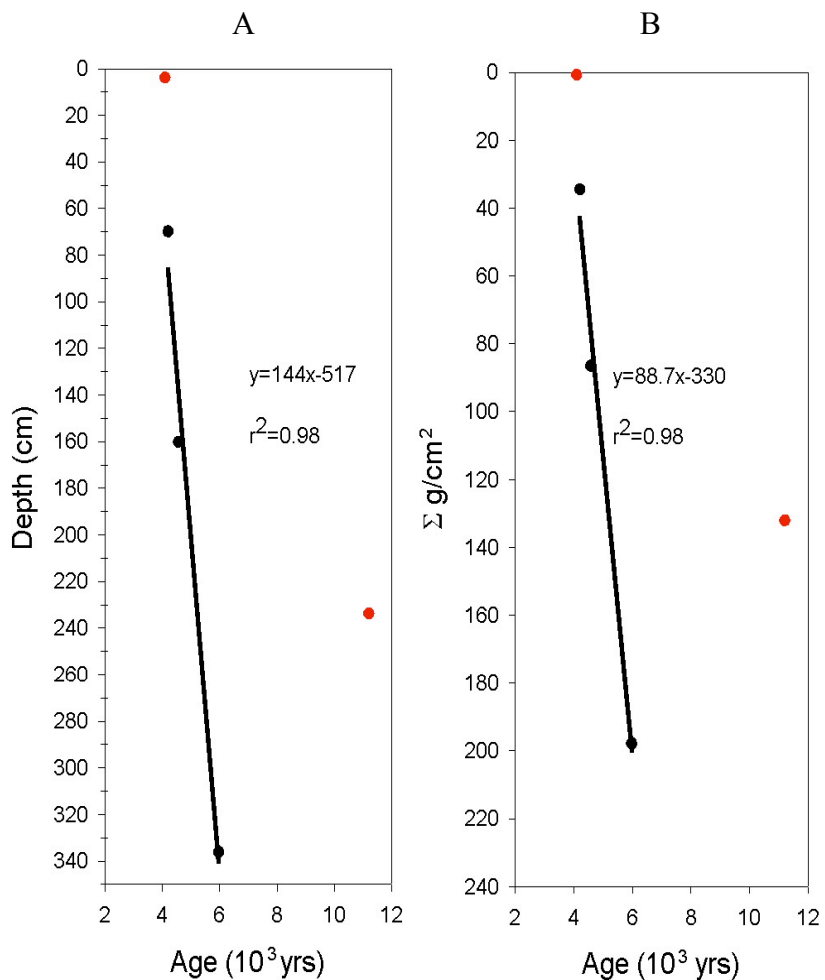


Figure 3.3. ^{14}C age of clay particles from the piston core are plotted with respect to depth (A), and Σ g/cm 2 (B). A linear regression was found in both instances and yielded rates of 0.14 cm/yr and 0.09 g/cm 2 /yr. Red dots are samples that were excluded from the regression because of bomb carbon influence or a clear outlying nature.

Previous studies conducted on the middle Eel shelf have found that flood layer deposits are preserved in the sedimentary record and play a large role in sediment accumulation rates (Leithold, 1989; Sommerfield and Nittrouer, 1999). By identifying discrete flood layers in the K70 piston core, which will be discussed later, and subtracting their thickness from the recovered core, an estimate of the background accumulation rates were calculated. The background accumulation rate for the upper 70 cm of the piston core was calculated to range between 0.90-1.4 cm/yr. To determine the background accumulation rates of the remainder of the piston core the ^{14}C ages of the wood and clay isolates were replotted against depth after subtraction of the flood layer thickness (Fig. 3.4). A constant background accumulation of 0.16 cm/yr ($r^2=0.97$) and 0.13 ($r^2=0.97$) was determined from the wood and clay isolates respectively. Thus background accumulation rates over the last 50 years were still found to be approximately 6-11 times faster than previous rates.

Grain Size

Grain size analysis of the piston core revealed a major change in shelf sediments with depth in the seabed. Down to a depth of ~60 cm, clays and medium-fine silts dominated the piston core sediments, with the mean weight percent of the <25 μm fraction being $60.3\pm 13\%$ ($n=10$). However, below 60 cm the coarse fraction (>25 μm) dominated sediment composition and the mean weight percent of the <25 μm fraction fell to $33.9\pm 8.5\%$ ($n=35$). Statistical analysis showed these two means to be unequal ($p=.001$). This transition from

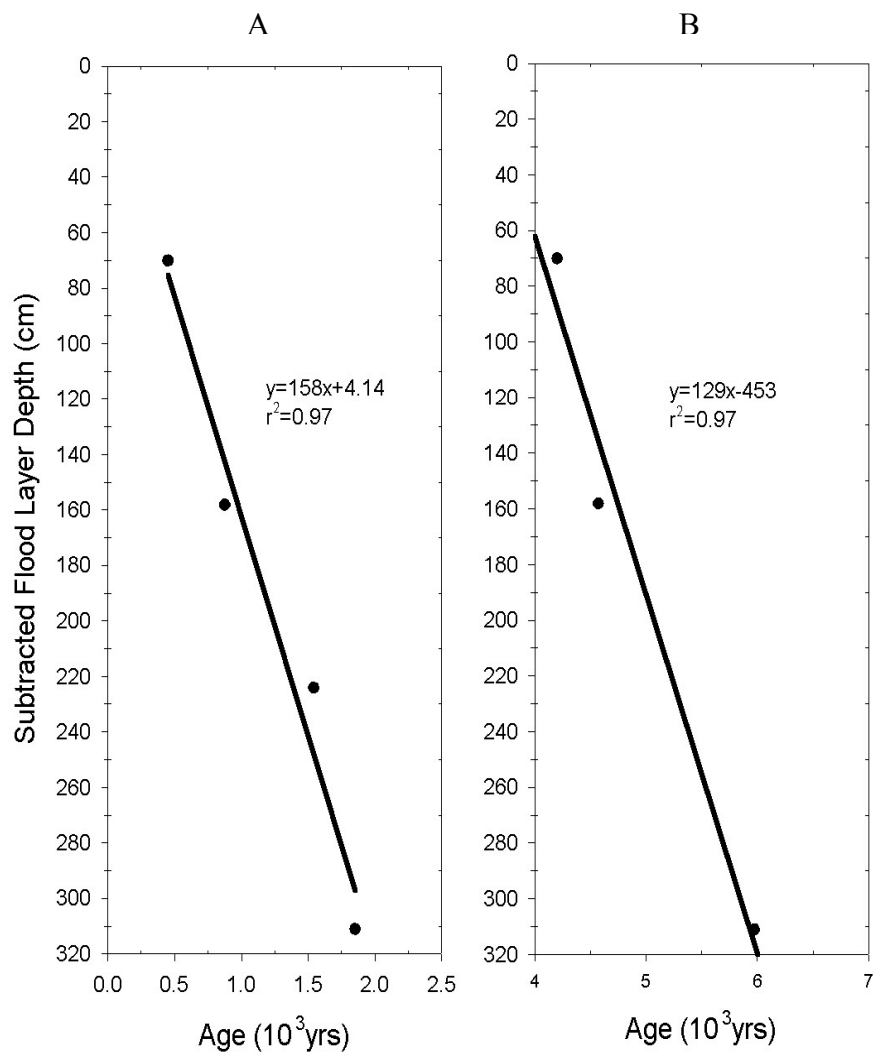


Figure 3.4. ¹⁴C ages of woody fragments (A) and clay particles (B) are plotted against depth down core after flood layer thickness had been subtracted. A linear regression was found in both instances and yielded background accumulation rates of 0.16 cm/yr (A) and 0.13 cm/yr (B).

finer to coarser sediment has been documented at similar depths in other studies conducted at K70 (e.g., Sommerfield, 1997 and Creamer, 1998; Sommerfield et al., 2002).

A higher resolution grain size analysis conducted on 5 samples showed the same trend in grain size with depth (Table 3.1). The samples in the upper 60 centimeters showed a mean grain size of $23.5 \pm 2 \mu\text{m}$, while the three samples below 60 centimeters had a coarser mean grain size of $39.3 \pm 11 \mu\text{m}$. While overall grain size increased with depth, the clay fraction ($<4 \mu\text{m}$) appeared to become finer with depth (Fig 3.5).

Several discrete layers of finer sediment were found in both cores. Previous studies have shown these layers of fine sediment to be dominated by clays and fine silts, and have interpreted them as historic flood deposits (Leithold, 1989; Creamer, 1998; Sommerfield and Nittrouer, 1999; Leithold and Blair, 2001). There were only two fine layers in the piston core with clay content greater than 20% (37 cm and 60 cm). The remainder of the core demonstrated consistent clay content that generally ranged between 10%-15% by weight. Therefore, flood layers in the piston core were identified by an increase in the medium-fine silt and clay fraction ($<25 \mu\text{m}$). In this study a flood layer was identified by the presence of a relative peak in $<25 \mu\text{m}$ sediment when compared to grain size data directly above and below the depth interval in question. Many of the fine-grained flood layers corresponded with regions of lower density (Fig. 3.6). This connection between low density and fine grain size was used to confirm the identification of flood layers in the upper 180 cm of the piston core.

Table 3.1. Results of a detailed grain size analysis of five samples from the K70 piston core. Mean grain size and % sand was found to increase with depth.

	26 cm	48 cm	212 cm	234 cm	296 cm
Median ϕ (ϕ m)	5.3 (25)	5.5 (22)	5.15 (28)	4.3 (51)	4.6 (41)
Mean ϕ (ϕ m)	6.27 (13)	6.37 (12)	6.05 (15)	4.98 (32)	5.3 (25)
% Sand	1.5	1.8	20.3	17.8	22.2
% Silt	78.8	69.7	57.5	69	65.4
% Clay	19.7	28.5	21.2	13.2	12.4

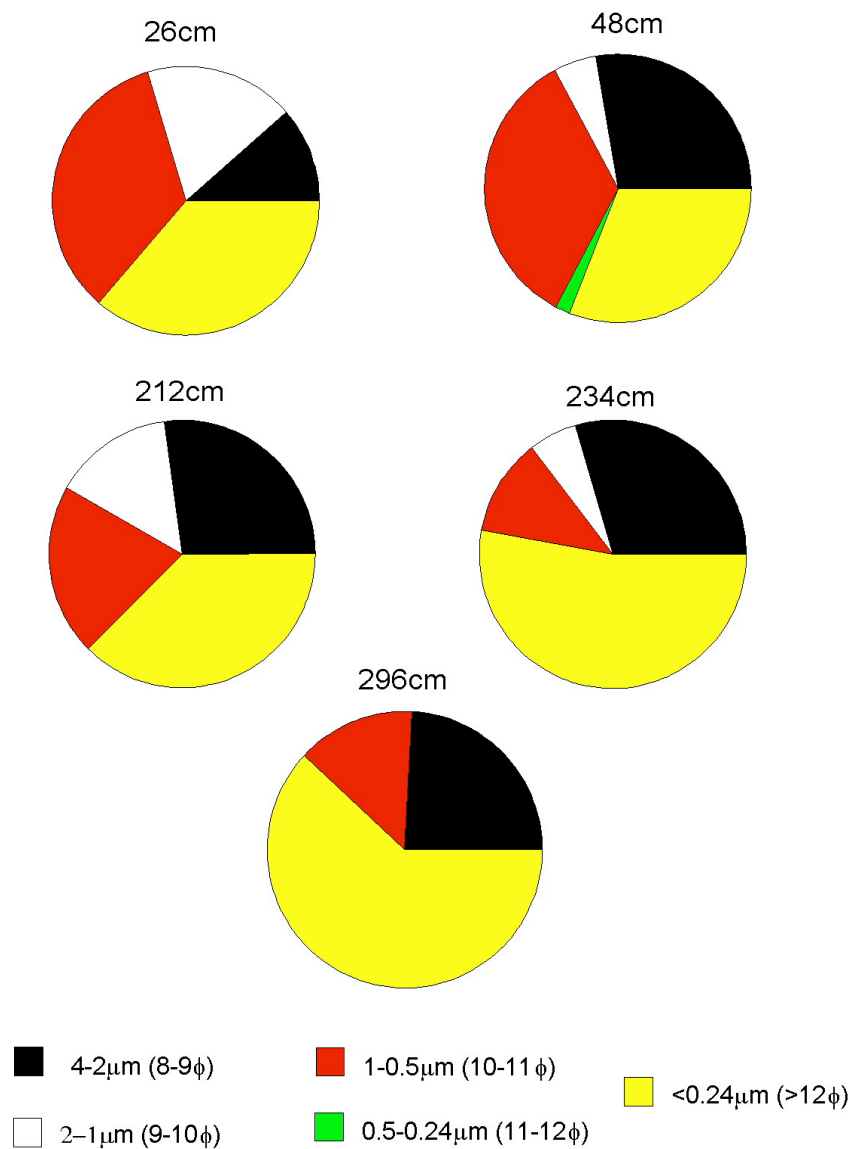


Figure 3.5. Pie charts showing the weight % distribution of the clay fraction for the five samples selected for detailed grain size analysis.

Clay grain size appears to decrease with depth.

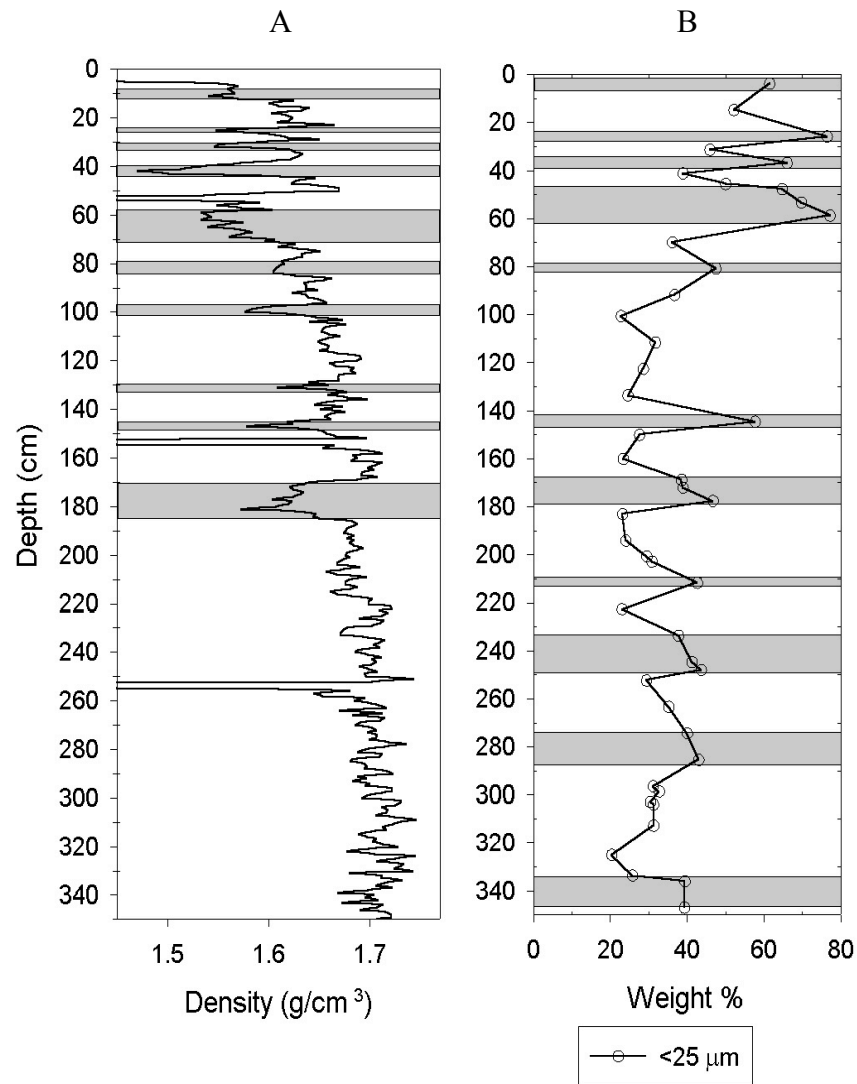


Figure 3.6. Plots of density (A) and grain size (B) from the K70 piston core. Above a depth of 180 cm the shaded regions of finer sediment in B correspond with shaded regions of low density in A. The correlation of these layers is not exact because of error involved in slicing the piston core at 1 cm intervals. Plotted depths in B are corrected estimates.

Below 180 cm depth density difference between flood and non-flood sediments could not be observed. This could be due in part to compaction and dewatering of sediments with increased depth, or to the deposition of coarser flood layers in the past.

Because piston corers typically disturb surface sediment, a box core was recorded at the same locality to obtain a less disturbed sample of the upper portion of the seabed. The cores were compared by matching various flood layers based on the grain size data and depth (Fig. 3.7). While there is some offset in depth and grain size distribution, a reasonable comparison between the two cores can still be made. Therefore the box core was used to get a clearer picture of the surface record at K70. Density and grain size results from both the box and piston cores indicated that there are 7 flood layers preserved above 60 centimeters, and 7 flood layers below.

Organic Carbon

Organic analyses of bulk, coarse silt and sand ($>25 \mu\text{m}$), medium-fine silt ($4\text{--}25 \mu\text{m}$), and clay ($<4 \mu\text{m}$) fractions were run on the same six samples selected for ^{14}C analysis. While grain size results and the ^{14}C age of woody fragments showed a distinct difference between shallow and deep sections of the piston core, the nature of organic matter in the different size fractions of these samples remained fairly constant with depth (Fig. 3.8). When the mean values of atomic C/N, weight %OC, and $\delta^{13}\text{C}$ for samples shallower than 60 cm depth were compared to the means below 60 cm depth no statistical difference was

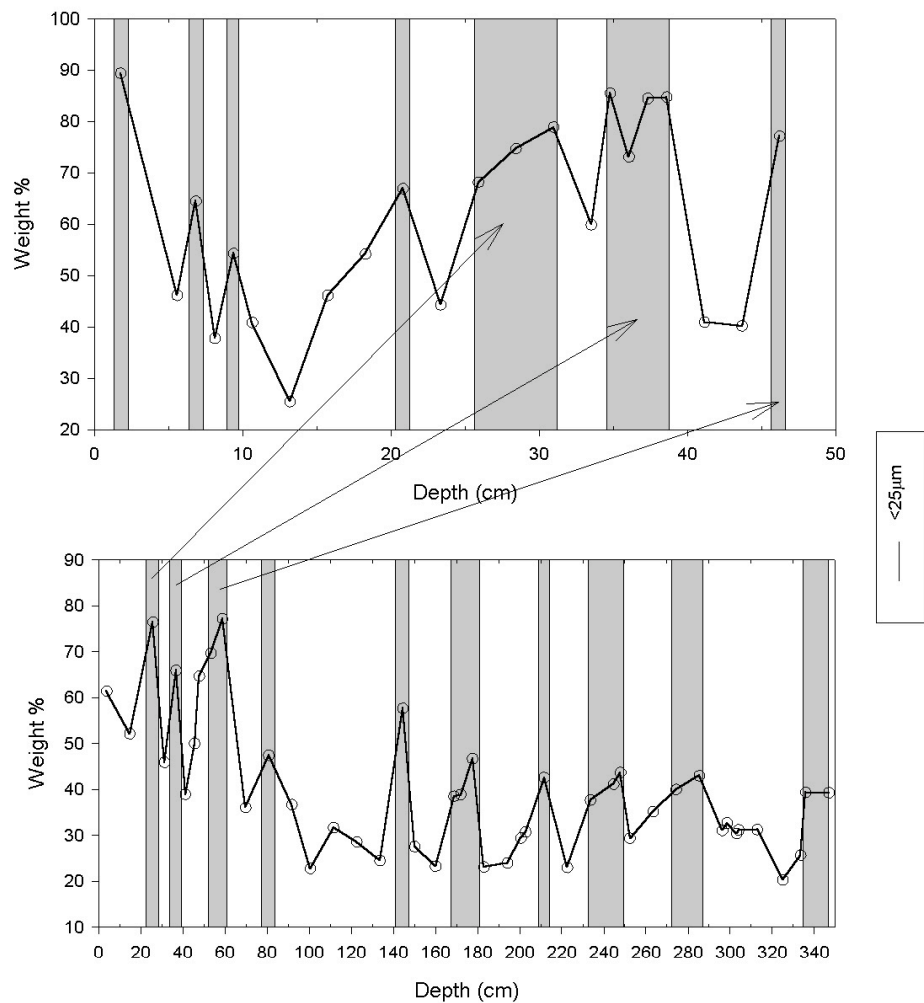


Figure 3.7. Comparison of flood layers between the box core and piston core from K70. Arrows indicate flood layers that match approximate depth and grain size between the two

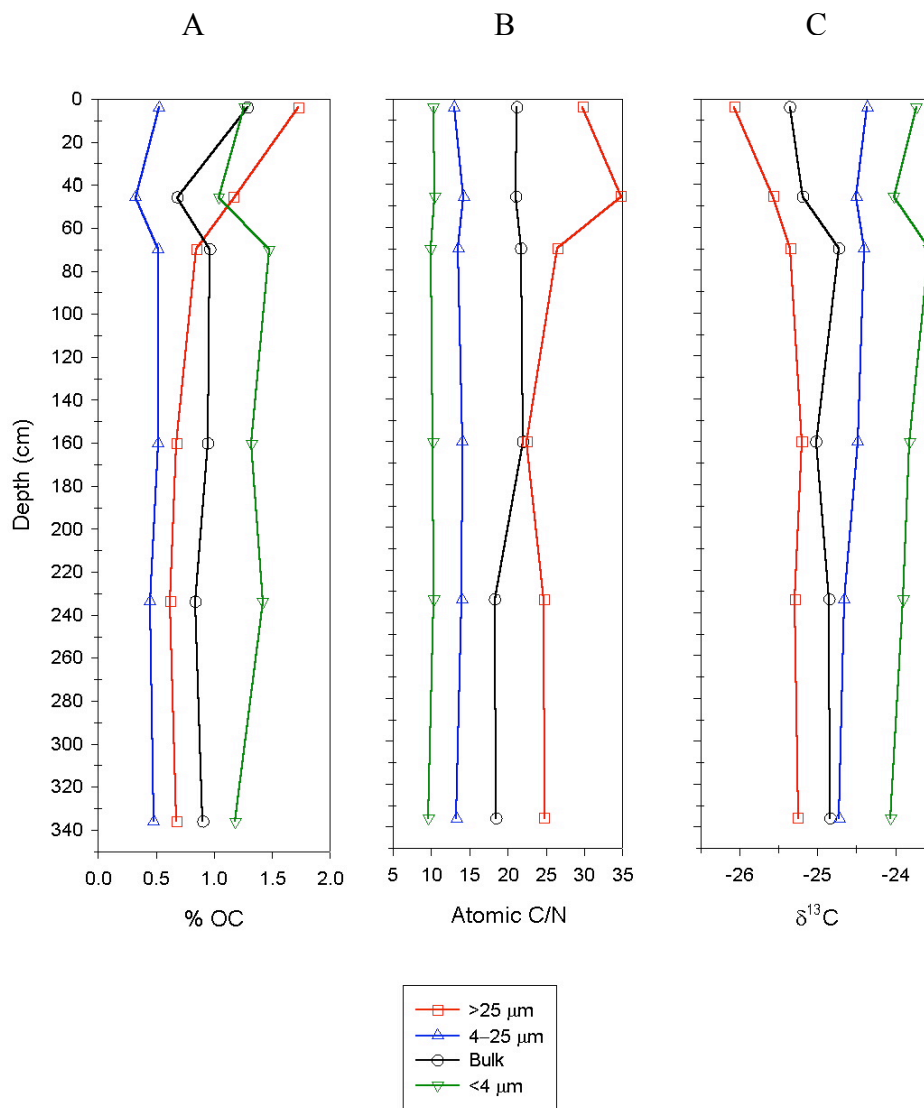


Figure 3.8. Plots of weight %OC (A), atomic C/N (B), and $\delta^{13}\text{C}$ (C) are shown for the fractions of the piston core. The >25 μm fraction shows downcore change in its C/N ratio and weight %OC. The >25 μm fraction also has the highest C/N ratios and most depleted $\delta^{13}\text{C}$ values, while the clay fraction has the highest $\delta^{13}\text{C}$ values and the lowest C/N ratios.

determined at the 5% significance level for all size fractions. This result is due in large part to the small population sizes being analyzed ($n=2$ and $n=4$; Rao, 1998). When the organic carbon data from the four size fractions was plotted versus depth (Fig. 3.8) changes in the nature of the organic carbon associated with the coarse fraction could be seen.

The coarse fraction showed an apparent decrease in %OC with depth. Samples above 60 centimeters had a mean weight %OC ($1.5 \pm 0.4\%$) that was approximately twice the mean of samples below 60 cm ($0.71 \pm 0.1\%$). This coarse fraction also had a higher mean atomic C/N ratio for depths shallower than 60 centimeters (32.3 ± 4) than below (24.6 ± 2). The $\delta^{13}\text{C}$ versus depth (Fig. 3.8) also indicated a downcore enrichment of ^{13}C relative to ^{12}C .

Differences in organic carbon between the size fractions were also examined for the six samples. For all depths it was found that the clay fraction had the lowest C/N ratios while the coarse fraction had the highest ratios. The $\delta^{13}\text{C}$ data also showed these same fractions to be the extremes, with the clay being the most enriched and the $>25 \mu\text{m}$ being the most depleted in ^{13}C (Fig. 3.8). The medium-fine silt fraction had the lowest weight %OC for all depths.

The distribution of total organic carbon through the three size fractions was determined for these six samples. Recovery of the organic carbon after grain-size separation was first calculated by comparing the mass balanced OC contents of the individual size fractions ($>25 \mu\text{m}$, $4-25 \mu\text{m}$, and $<4 \mu\text{m}$) to the unfractionated bulk samples for all depths. The recovery of organic carbon ranged from 74%-120%, with no observable shift in $\delta^{13}\text{C}$ (Table 3.2). A budget

Table 3.2. A budget of the weight percent organic carbon for each size fraction. Organic carbon recovery after fractionation ranged from 74%-120%. Despite the wide range of recovery, $\delta^{13}\text{C}$ values of bulk samples are near identical to the summed $\delta^{13}\text{C}$ of the resulting fractions. A budget of the recovered organic carbon shows that the majority of the OC is from the >25 μm fraction.

	4 μm	46 μm	70 μm	160 μm	234 μm	336 μm
Weight %OC (bulk)	1.3	0.68	0.96	0.95	0.84	0.90
Weight %OC (calculated)	1.03	0.82	0.81	0.70	0.63	0.69
%OC recovered	80	120	84	74	79	76
%OC >25 μm	52.5	74.2	64.1	69.2	55.9	60.3
%OC 4 μm -25 μm	26.0	15.4	18.4	14.2	19.7	18.4
%OC <4 μm	21.5	10.4	17.5	16.6	24.4	21.3
$\delta^{13}\text{C}$ (bulk)	-25.3‰	-25.2‰	-24.7‰	-25.0‰	-24.8‰	-24.8‰
$\delta^{13}\text{C}$ (calculated)	-25.1‰	-25.2‰	-24.9‰	-24.9‰	-24.8‰	-24.9‰

of the mass balanced total %OC showed that the majority (53-74%) of the organic carbon recovered was located within the coarse fraction. When viewed under a microscope large amounts of discrete, woody pieces not bound to particles were seen in this fraction.

An examination of the mineral-bound organic carbon was of key interest in this study. Previous studies have indicated that the majority of sedimentary organic carbon associated with particles is found within the fine, clay fraction (e.g. Keil et al., 1994; Mayer, 1994a,b; Ransom et al., 1998; Bock and Mayer, 2000). Therefore, the majority of organic analyses performed on sediments from K70 were performed on clay isolates.

Weight percent organic carbon of the clay fraction from the piston core ranged from \square 0.9%-1.5%, and the mean %OC for samples above 60 cm ($1.05\pm 0.1\%$, $n=8$) was statistically different than the mean below 60 cm ($1.3\pm 0.1\%$, $n=30$, $p=.001$). The mean %OC above 60 cm was approximately 80% of the mean below. A similar trend was observed in carbon loading (OC/SA) of clay particles at K70. Shallow samples had a mean OC/SA ratio that was statistically lower ($\approx 30\%$) than samples below 60 cm depth ($p=.001$, Fig. 3.9). The $\square^{13}\text{C}$ values of the clay fraction ranged from -24.5‰ to -23.5‰ , and the mean above 60 centimeters ($-24.1\pm 0.3\text{‰}$) was found to be indistinguishable from the mean below 60 centimeters ($-23.8\pm 0.2\text{‰}$, $p=.001$). While a large difference in the isotopic signature of the clay fraction was not observed downcore, it was found that the most negative $\square^{13}\text{C}$ values were associated with the two layers with

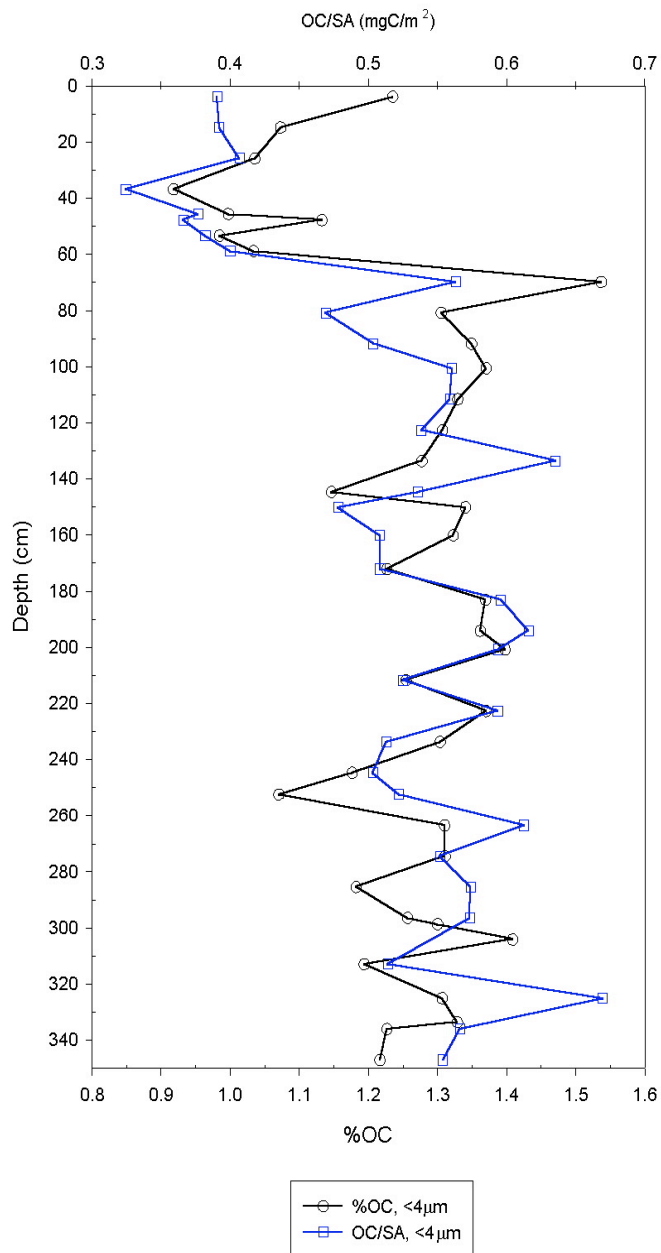


Figure 3.9. Plot of weight %OC and carbon loading for clays from the piston core at K70. A small shift from lower to higher weight %OC and carbon loading is found in the piston core just below 60 cm.

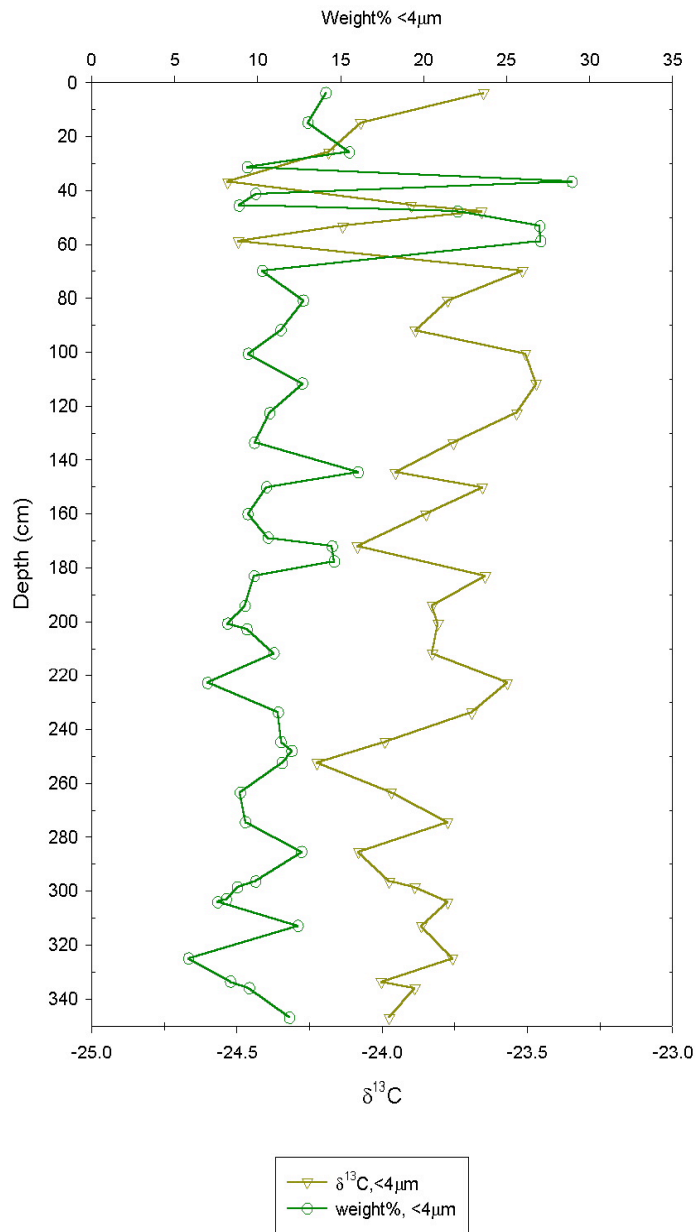


Figure 3.10. Plots of weight % and $\delta^{13}\text{C}$ values of the clay fraction are shown for the K70 piston core. The two regions of the core with high clay content (37cm and 60cm) are associated with areas where the $\delta^{13}\text{C}$ value becomes more depleted in ^{13}C .

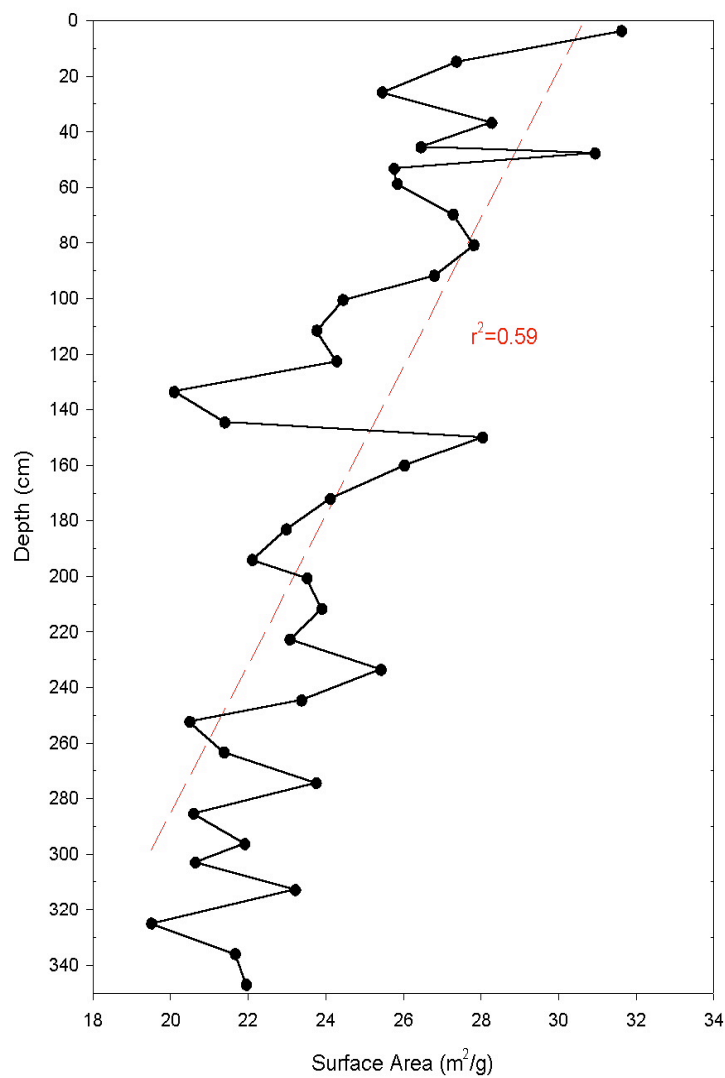


Figure 3.11. Plot of surface area of the clay fraction from the K70 piston core.

The surface area profile illustrates the correlation between clay surface area and depth. The clay surface area decreases with increasing depth downcore.

clay content greater than 25% by weight in the upper 60 cm of the core (Fig. 3.10).

Surface Area

Surface area values of the clay isolates from the K70 piston core ranged from 19.5m²/g to 31.6m²/g. As with the organic carbon measurements, average surface area above 60 cm was compared to the average below. Statistical results showed that the mean surface area above 60 cm was higher than below (p=.001). However, when surface area was plotted against depth (Fig. 3.11) it was found that an overall increase in depth correlated with a decrease in the surface area of clay particles ($r^2=0.59$).

Clay Mineralogy

The X-ray diffractograms indicated that the clay fraction was composed of chlorite, illite, smectite, quartz, and possibly vermiculite, and that this composition was constant for all treatments and depths at K70. Diffractogram patterns showed peaks in areas that suggest a presence of chlorite and illite in the clay fraction (Fig. 3.12; Moore and Reynolds, 1989). Confirmation of the presence of chlorite was obtained by the increase of relative intensity seen in the 6° 2θ peak for K-saturated slides heated to 550°C (Fig. 3.13). The presence of this peak at 550°C also excluded kaolinite from being a major component in the clay mineralogy (Moore and Reynolds, 1989). The expansion of the 6° 2θ peak to the 5-6° 2θ region upon exposure to ethylene glycol after Mg-saturation indicated the presence of smectites (Fig. 3.14). Confirmation of the presence of

smectite was seen in the collapse of the $6^\circ 2\theta$ peak to $8.7^\circ 2\theta$ when K-saturated slides were heated to 300°C (Figs. 3.12 and 3.13; More and Reynolds, 1989). When a comparison of relative intensities was made between the air-dried Mg-saturated slides and the air-dried K-saturated slides this same collapse from 6° to $8.7^\circ 2\theta$ was seen. The increased relative intensity of the $8.7^\circ 2\theta$ peak after K-saturation and without heating suggested the possibility of a vermiculite component to the clay mineralogy (Walker, 1957). Evidence for quartz was determined through the presence of peaks at $21^\circ 2\theta$ and $26.7^\circ 2\theta$ (Moore and Reynolds, 1989). A quantitative analysis of the mineralogy was not performed in this study, however consistent relative intensity peak heights for all samples suggests that no large scale change in percent mineral composition occurs in the core.

During the period of usage a maintenance check and professional recalibration of the XRD was made. This maintenance and calibration resulted in higher intensity returns on the diffractograms and a positive 2θ shift of about 0.3° . An internal standard of quartz revealed that the peak positions prior to the recalibration were more accurate than positions after recalibration. Because of an increase in intensity, slides were rerun after the calibration to allow for clearer diffractograms to be presented. The K-saturated, air-dried sample from 5.5 centimeters depth was not rerun due to lack of material, and therefore illustrates this 2θ shift and increased noise in its diffractogram (fig. 3.12). The diffractograms were not corrected for this shift because the $0.3^\circ 2\theta$ offset was not constant for the duration of each scan.

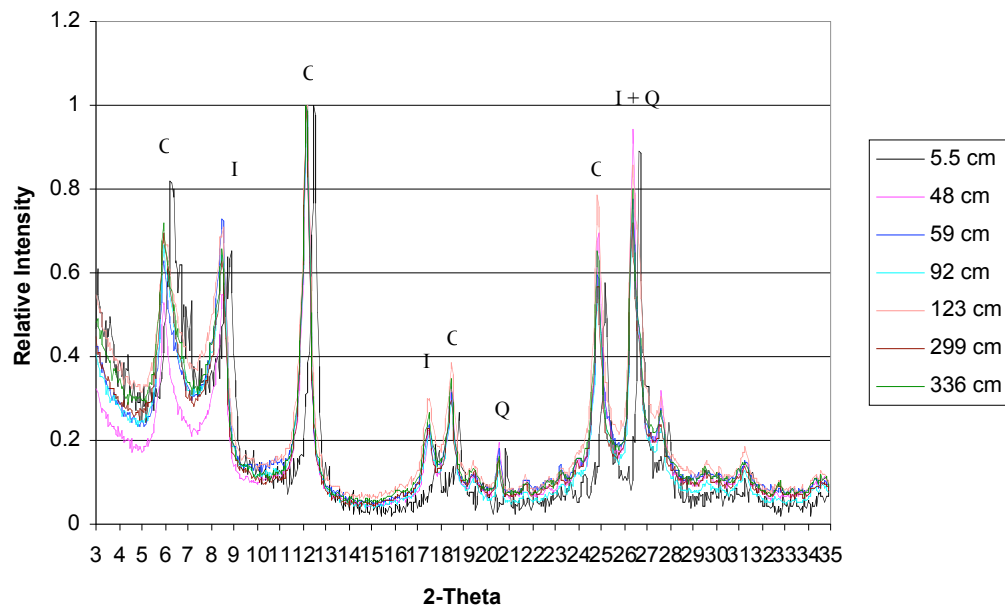


Figure 3.12. Diffraction patterns for K-saturated air-dried samples. Peaks are labeled for chlorite (C), illite (I), and quartz (Q). A positive shift of $0.3^\circ 2\theta$ is seen for the 5.5 cm K-saturated diffraction above due to recalibration of the XRD. Despite this shift, a general consistency of peak positions and relative peak heights are seen for all the K-saturated samples.

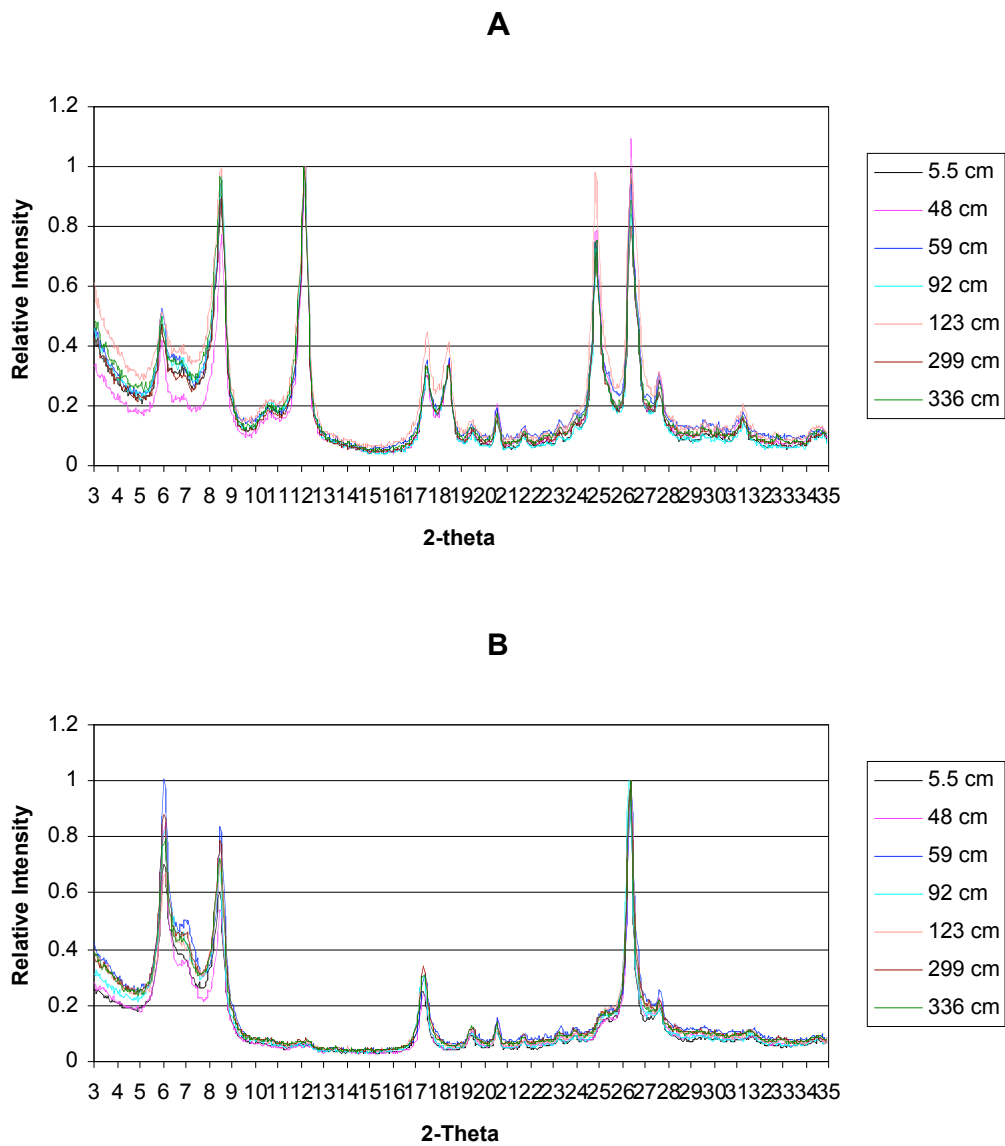


Figure 3.13. X-ray diffractograms of K-saturated samples heated to 300°C (A) and 550°C (B). The peak shift from 6° 2 θ to 8.7° 2 θ when heated to 300°C suggests the presence of smectites. The presence of a 6° 2 θ peak after heating to 550°C eliminates kaolinite from being a major component. A consistent relative peak height and location is seen for all samples in both treatments.

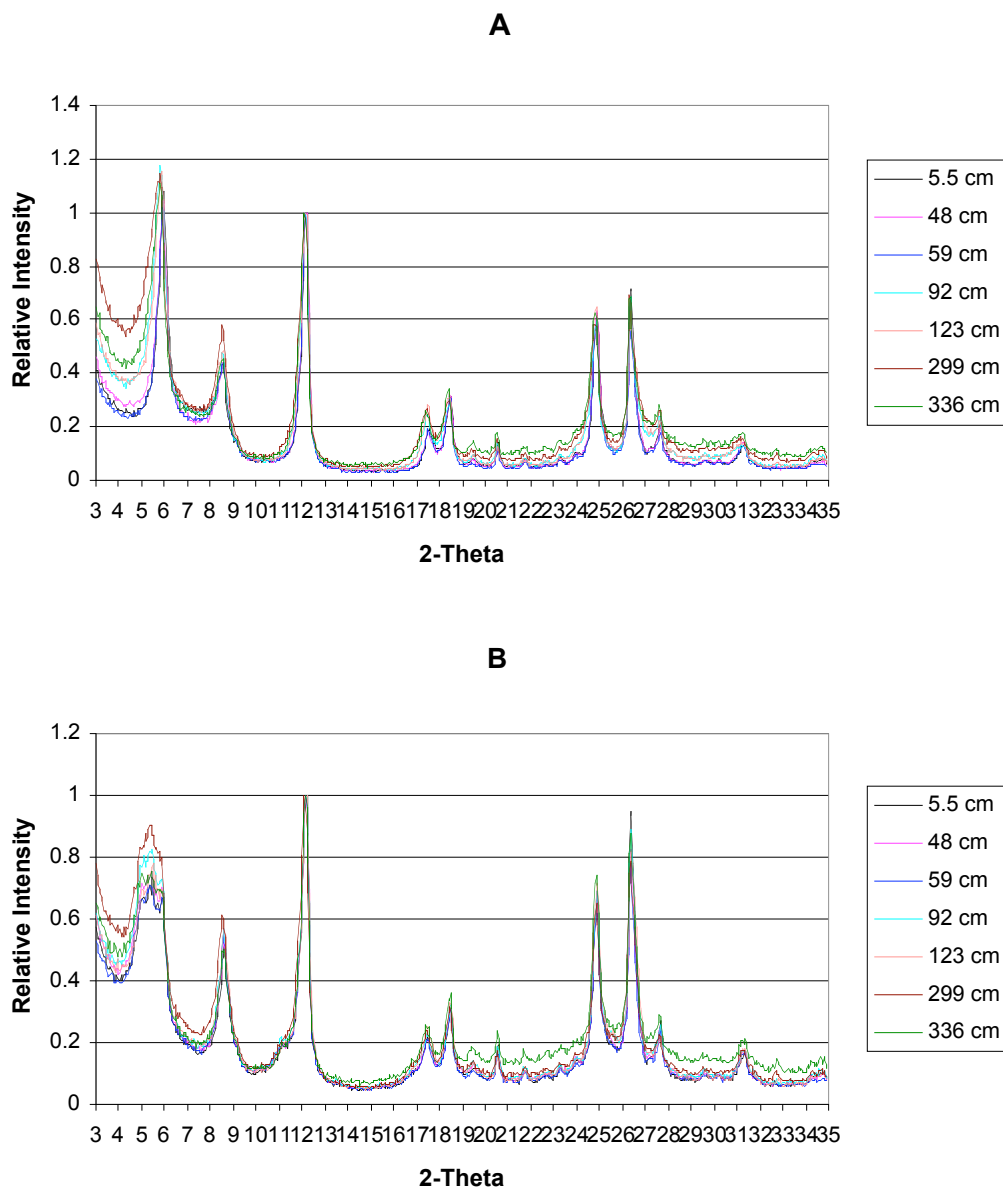


Figure 3.14. X-ray diffractograms of Mg-saturated slides (A) and Mg-saturated slides exposed to ethylene glycol (B). All samples show consistent peak positions and relative intensities for both treatments. Broadening of the $6^\circ 2\theta$ peak after ethylene glycol exposure confirms the presence of expandable clays (smectites).

4. Discussion

Shelf Sediments

Examination of the cores from K70 reveals that sedimentation processes on the Eel Shelf have not been constant over the historic past. The $\delta^{14}\text{C}$ of discrete woody pieces and clay particles indicates rapid recent accumulation rates, but reduced, constant accumulation rate for sediments below a depth of 70 centimeters (Figs. 3.4). Prior studies (e.g. Sommerfield and Nittrouer, 1999; Sommerfield et al., 2002) have used ^{137}Cs data to document decreased accumulation rates on the Eel shelf after about 1954. A study by Creamer (1998) showed that this change in accumulation rate coincided with deposition of a thick flood layer (approx. 10 cm) and a downcore coarsening in grain size preserved at a depth of 55-65 cm in a kasten core recovered from K70 in 1995. Analysis of the K70 piston core in this study revealed a similar change from finer to coarser sediments at 60 centimeters depth. A flood layer in the piston core was also located in this approximate interval (48-59 cm) (Fig. 3.6). This is interpreted to be the same flood layer that has been attributed to the historic 1955 flood in other studies based on maximum ^{137}Cs penetration (Creamer, 1998; Sommerfield and Nittrouer, 1999). The post-modern ages of woody pieces found above 70 cm depth in the piston core demonstrates exposure to bomb carbon, and therefore indicates that this part of the core is no older than the middle 20th century. However, because diffusion of ^{137}Cs in the sediment column is possible, the dating of this depth to 1955 may not be exact (Beasley et al., 1982). Historical records indicate that the two largest flood events of the past century occurred in

1955 and 1964 (Syvitski and Morehead, 1999), and the 48-59 cm flood deposit in the K70 piston core could be an amalgamated deposit from both events.

Therefore, in this study, this flood layer is attributed to a period between 1955-1964.

Dating of the floods above the 1955-1964 horizon was based on the estimated background accumulation rate for the upper region of the piston core (0.90-1.4 cm/yr). The approximate time frame of deposition for the 7 flood layers identified in the box core is illustrated in Figure 4.1. These estimated dates of deposition agree with historical records of Eel River floods. The lowermost flood layer in the box core, located at 46 cm depth, was dated to a time period between the 1940's-1960's. The depth of this flood layer corresponds to the start of the 1955-1964 period in the piston core (48 cm), and therefore is likewise estimated to mark the 1955-1964 period. Due to overlapping age estimations, both the 35-39 cm deposit and the 26-31 cm layer could be correlated to either historic floods in 1969 and 1974 (Creamer, 1998; Syvitski and Morehead, 1999). The increase in grain size and density between the layers suggests that these are two different flood events, but a definitive correlation to a historic flood could not be made. The flood layer located at 21 cm depth could also be associated with the 1974 flood, but more likely corresponds to documented floods that occurred in 1982 or 1986. The remaining three flood layers found at 9, 7, and 2 centimeters depth in the core are attributed floods that occurred in 1993, 1995, and 1997, respectively (Creamer, 1998; Syvitski and Morehead, 1999; Wheatcroft and Borgeld, 2000).

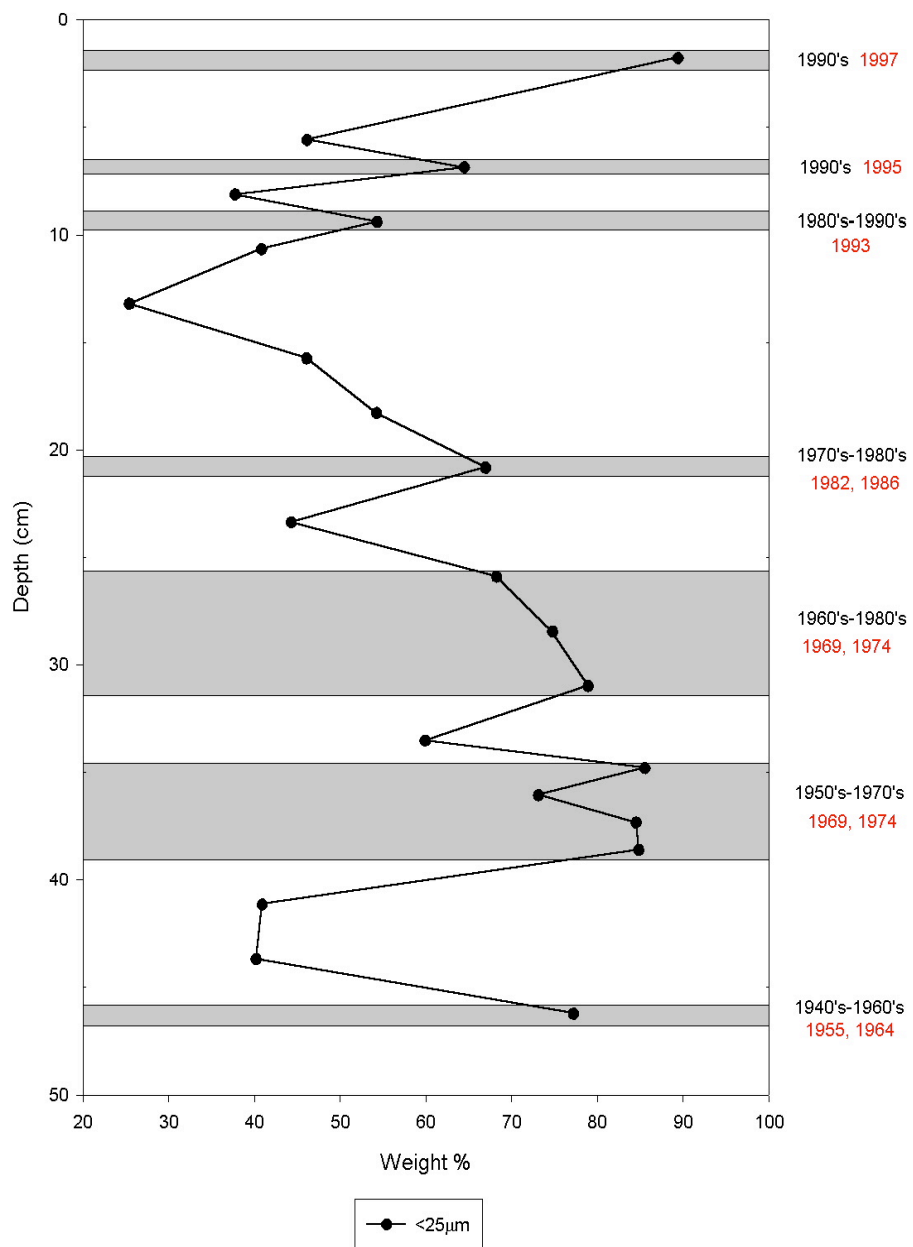


Figure 4.1. Flood layers from the K70 box core. Approximate time frames of deposition based on accumulation rates are indicated in black numbers.

Historically documented floods that are proposed to be responsible for these flood layers are indicated in red numbering.

Below the 1955-1964 flood layer the average background sediment accumulation rate of 0.15 ± 0.02 cm/yr obtained from the ^{14}C data of clay particles and woody debris was used to date various levels in the piston core. The bottom of the core was estimated to be just less than 2000 years old. Reasonable agreement with this accumulation rate over a similar time span was found in a previous study (Sommerfield et al., 2002). The Sommerfield et al. study found ^{14}C -based accumulation rates to range between 0.1-0.5 cm/yr for a period from A.D. 400-1954 at a nearby location on the shelf (O70).

The estimated time frame of deposition for the seven flood layers below 60 cm depth in the piston core is illustrated in figure 4.2. As with the more recent flood layers, historical records along with measured water discharge levels were examined in an attempt to find supporting evidence for floods that correspond to the assigned time periods. Historical records of floods in the watershed document three major floods that occurred in 1861, 1881, and 1890 (Helley and LaMarche, 1973). Any or all of these could be responsible for the flood layer located at 81 cm depth downcore.

Because records of water discharge of the Eel River only date back to 1911, direct measurements of discharge could not be used to identify periods of high flow for the entire core. Discharge records of the Sacramento River near Red Bluff, CA, however, were found to correlate with discharge levels of the Eel River ($r^2=0.82$, Fig. 4.3). Therefore, reconstructed discharge levels of the Sacramento River based on tree ring data (Meko et al., 2001a) were used to

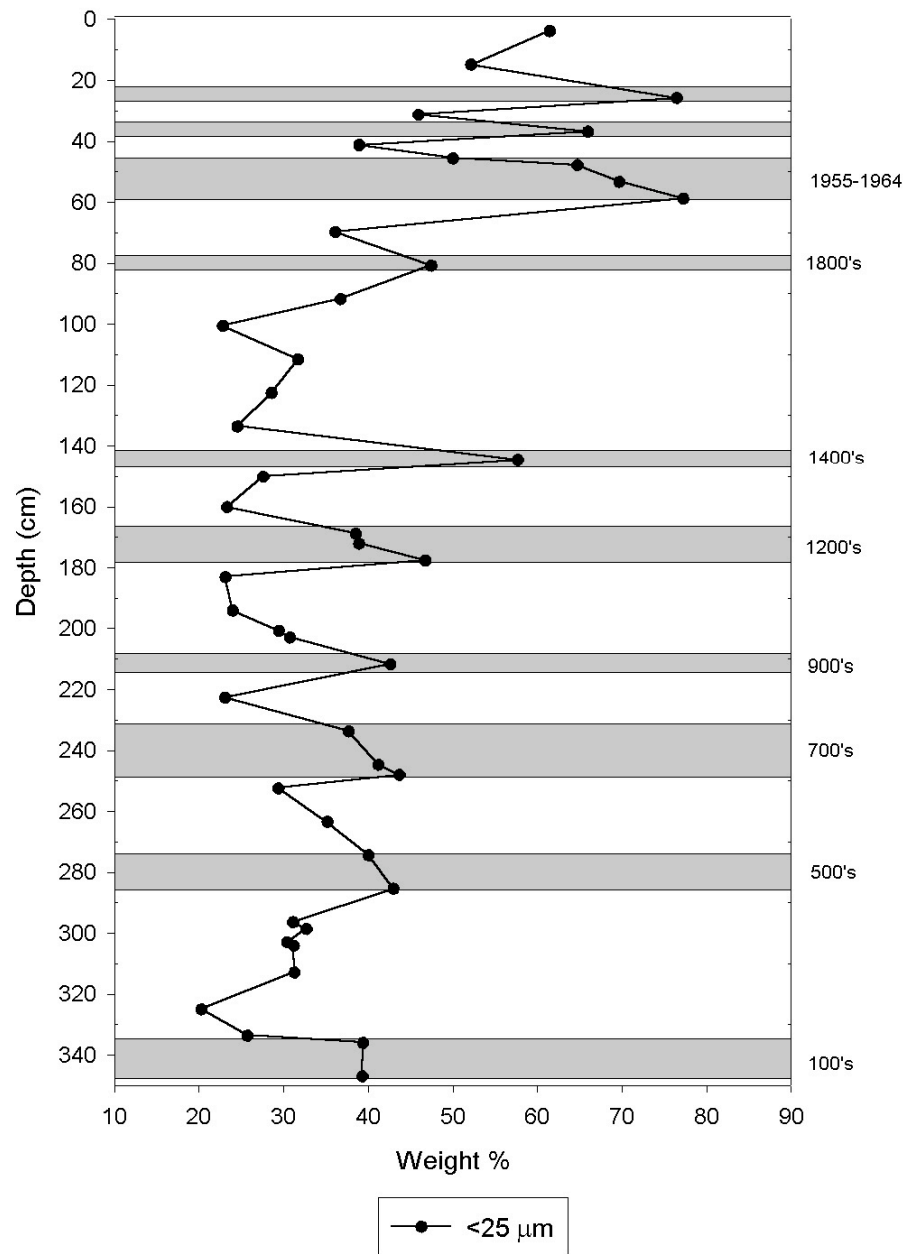


Figure 4.2. Flood layers from the K70 piston core. Approximate time frames of deposition for flood layers below the 1955-1964 horizon were obtained by using a constant accumulation rate of 0.15 ± 0.02 cm/yr.

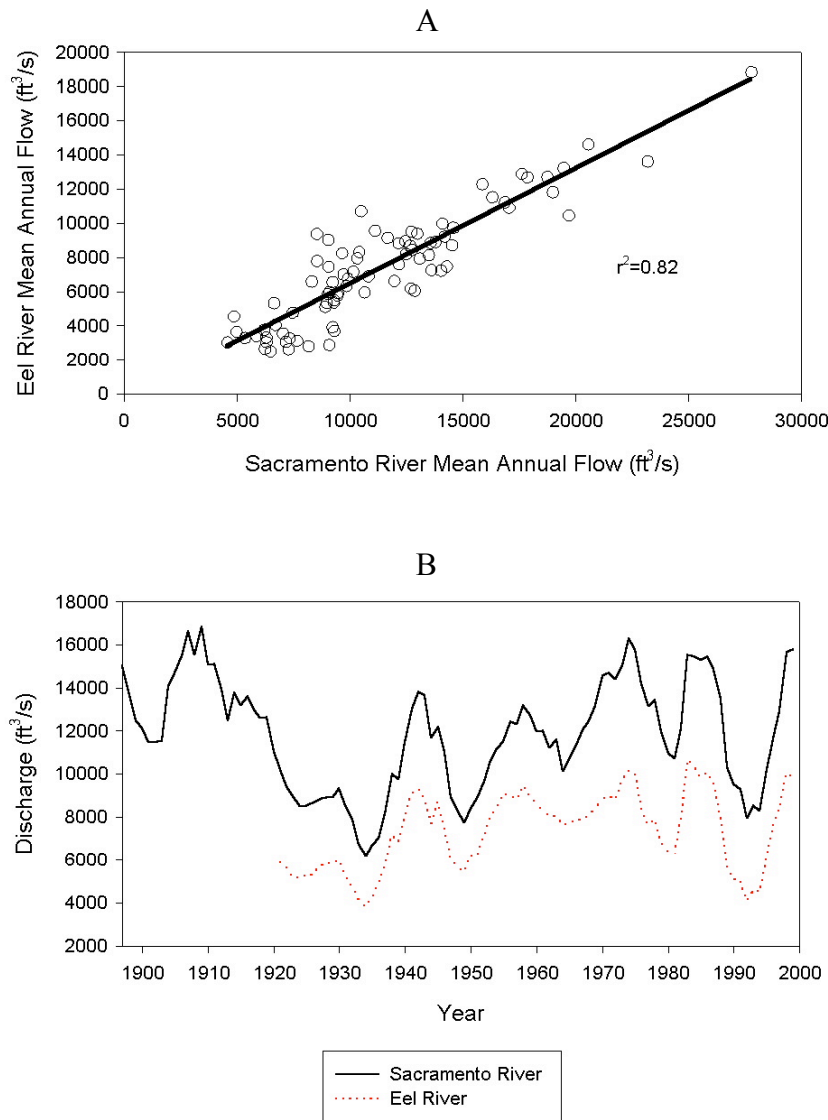


Figure 4.3. Plotted mean annual discharges of the Eel River at Scotia and Sacramento river near Red Bluff show that reasonable correlation can be made between the two river systems (A). The 6 year running mean discharge record shows that the Sacramento River has higher discharge levels, but that time periods of high and low discharge of the two rivers coincide (B).

identify generally wet intervals of time within the Eel River basin. The flood events in the 1400's (145 cm downcore), 1200's (169-178 cm downcore), and 900's (212 cm downcore) correspond with periods of increased reconstructed discharge (Fig. 4.4). The remaining flood layers below the 1955-1964 horizon predated the tree ring data from the Sacramento River. The reconstructed Sacramento River record provides the means for identifying wet intervals of time, but it does not necessarily record storm events. For example, some historically documented floods of the Eel River (e.g. 1890 and 1964) do not match up with periods of highly elevated annual discharge of the Sacramento River (Fig. 4.4). Provided that the remainder of the year were relatively dry, however, it would be possible to have a high discharge flood event without raising the annual average discharge. Historical records indicate that this appears to have been the case for the December 1964 flood (Helley and LaMarche, 1973).

Geologic and botanical evidence has also been found for past Eel River floods dating to A.D. 1600 and 1750 (Helley and LaMarche, 1973). While there is a slight increase in the <25 μ m sediment content in the piston core that would approximately correspond with A.D. 1600 (114 cm downcore), there is no density log evidence to support the presence of a flood layer at this depth. No grain size or density log evidence was identified in the piston core that would correspond with a flood event around A.D. 1750 (92 cm depth). No data were collected from the exact depths that correspond to 1600 and 1750, and thus it is possible that thin, preserved flood layers were passed over during initial examination of the piston core. It has been shown that large magnitude floods of the Eel River

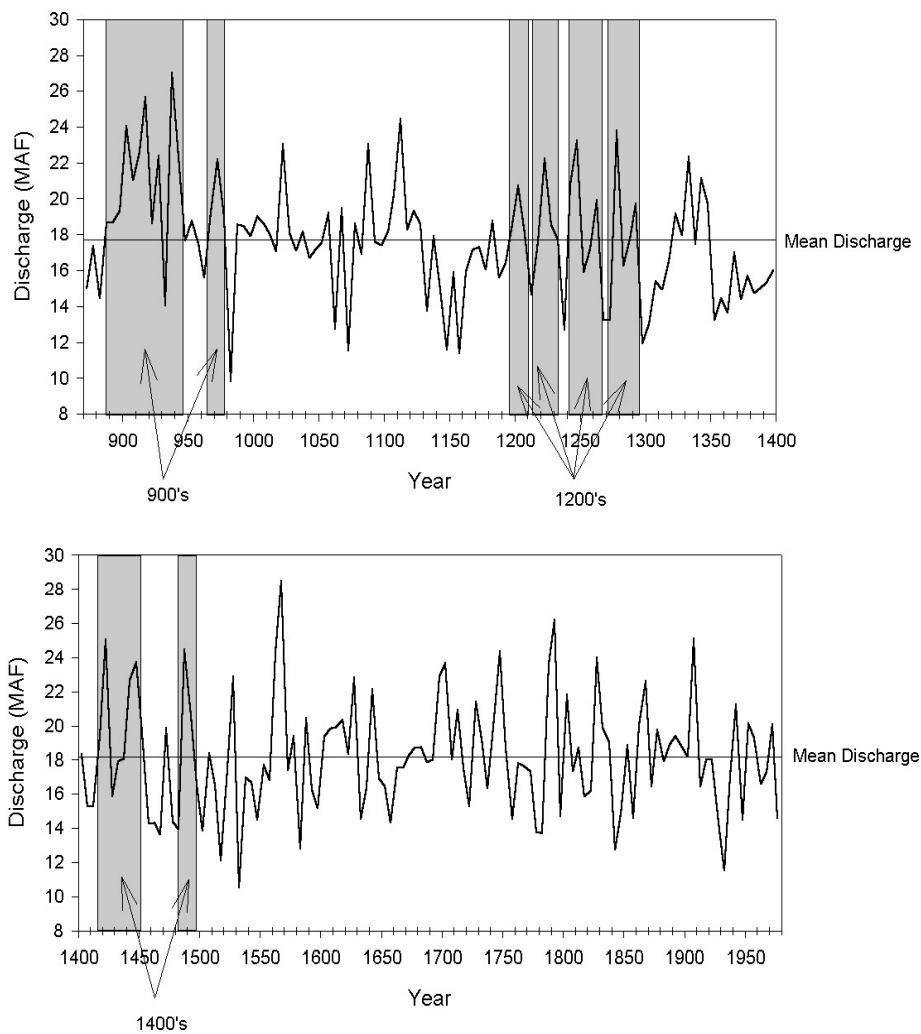


Figure 4.4. 6-yr running mean of reconstructed discharge (MAF) of the Sacramento River based on tree ring studies taken from Meko et al. (2001b). Shaded regions indicate elevated periods of wetness that correspond to approximate time periods of recorded floods in the K70 piston core. Note historically recorded floods from 1890 and 1964 do not correspond with elevated discharge.

do not always leave thick flood deposits (Wheatcroft and Borgeld, 2000).

Wheatcroft and Borgeld (2000) found that an 80-year flood event in 1997 did not leave a thick flood deposit on the middle Eel shelf, but was instead distributed in a thin layer over a large area.

A total of 14 flood layers were identified in the cores from K70, half occurring in the last 50 years. The remaining recorded flood events are distributed over a time period of approximately 1900 years. This change in apparent flood frequency has been cited as a reason for the change in accumulation rate and grain size at K70 (Creamer, 1998; Sommerfield et al., 2002). Since it has been documented that most of the sediment discharged by the Eel River is associated with flood events, it stands to reason that a decrease in flood frequency would result in a decrease in sedimentation rates (Brown and Ritter, 1971). Past explanations for the downcore decrease in flood frequency have focused on lower storm frequencies in the region prior to the middle 1900's (Creamer, 1998; Sommerfield et al., 2002). An analysis of the U.S. Geological Survey discharge data for the Eel River at Scotia (1911-1999) showed that from 1999-1950 major floods (≥ 10 yr. recurrence intervals) were more than two times more frequent when compared to the previous 40 years (Sommerfield et al., 2002). As stated previously, reconstructed discharge data of the nearby Sacramento River was used to identify periods of wetness further back in time. The long-term record of discharge levels reconstructed for the Sacramento River, however, suggest that recent levels of precipitation and runoff are not unique in the past 1100 years (Fig. 4.4; Meko et al., 2001). Despite the fact that other

periods of elevated river discharge are indicated for this period, constant accumulation rates and grain size are recorded below 60 cm at K70. This observation implies that lower water discharge may not be solely responsible for the slower sediment accumulation before the mid 1950's.

Changes in precipitation and river discharge are not the only perturbations the Eel River basin has seen over the last 50 years. Significant anthropogenic land use alteration also has occurred over the past few decades. After World War II, technological advances made development of the steep-sloped Eel River basin more economically feasible (Hackett, 1999). Stands of timber that were inaccessible before could now be harvested, resulting in timber production in the region reaching its peak in the late 1950's (Hackett, 1999; U.S. Environmental Protection Agency, 1999). Studies conducted on the North Island of New Zealand, which shares a very similar geology and climate with the Eel, demonstrate that deforestation can be directly linked to increases in erosion rates (Foster and Carter, 1997; Page and Trustrum, 1997, Hicks et al., 2000, Page et al., 2000). Not only was a seven-fold increase in erosion rate observed in the studies, but the mechanism of erosion was also shown to change. After logging of the New Zealand forests, gully formation increased in grassland areas and replaced landslides as the major source of erosion in the catchments (Foster and Carter, 1997; Page and Trustrum, 1997, Hicks et al., 2000, Page et al., 2000). Kelsey (1980) documented this same type of gully formation in the Van Duzen River basin, a tributary of the Eel River.

Evidence connecting the changes in shelf accumulation rates to deforestation was seen in the ^{14}C ages of wood fragments from the K70 piston core. Pieces of coarse woody debris of Douglas Fir, a common tree species of the region, have been shown to persist on the forest floor for centuries (Sollins et al., 1987; Stone et al., 1998; Gavin, 2001). Therefore, under natural conditions these logs would continue to decay and provide a source of significantly aged wood to the watershed for several years after the tree's initial death. The fact that no evidence for old-growth pieces of wood was found above 70 cm depth in the piston core, i.e., they all gave post-modern ^{14}C dates, suggests that the source of aged wood debris was rapidly removed from the catchment. As stated earlier, industrial logging of the old-growth forests of the Eel River basin reached its peak in the late 1950's (Hackett, 1999). This time period corresponds to the depth where woody pieces transition from aged to post-modern, and where the sediment accumulation rate increases. The fact that prior studies have linked deforestation to elevated erosion rates in a similar basin, and that the height of industrial logging can be correlated to a depth where sedimentation rates changed, is consistent with a significant role of land use alteration in the increase of accumulation rates on the shelf after 1955-1964.

Organic Carbon of Shelf Sediments

While changes in grain size and accumulation rate on the middle Eel shelf have been previously recognized, no investigation has explored the effect of these changes on organic carbon burial. Statistical analysis of organic carbon associated

with bulk, coarse silt and sand, and medium-fine silt fractions of sediment revealed that the content, atomic C/N ratios, and isotopic signature of organic carbon associated with these sediments did not vary with depth. However, the organic carbon associated with the coarse (>25 μm) fraction displayed some noticeable changes when plotted against depth downcore. The mean weight %OC in this fraction above 60 cm was approximately twice of the mean weight %OC below the 1955-1964 horizon (Fig. 3.8). The decrease in organic carbon with depth was also associated with lower atomic C/N ratios and more enriched $\delta^{13}\text{C}_{\text{PDB}}$ values (Fig. 3.8). Such trends indicate that with depth less coarse terrestrial organic carbon, which tends to have lighter $\delta^{13}\text{C}$ values and higher C/N_a ratios (Fry and Sherr, 1984; Hedges et al., 1988; Goni et al., 1998), is found in the shelf environment. Other studies of shelf sediments have indicated that remineralization of terrestrial carbon is common in the marine environment (Aller et al., 1996; Keil et al., 1997). Recent studies, however, have suggested that some organic carbon can escape oxidation by being trapped in intra- or intergranular pores of clay minerals (Keil et al., 1994; Mayer, 1994a,b; Keil et al., 1997; Bock and Mayer, 2000). When viewed under a microscope, much of the organic material in this coarse fraction is from discrete woody fragments not directly associated with the mineral matrix. Organic matter of this size would be too large to be protected by intra- or intergranular pores of clay minerals, and thus would be more vulnerable to microbial attack resulting in rapid removal of terrestrial organic carbon.

While a case for diagenetic alteration of organic carbon can be made for the coarse fraction, it should be noted that the downcore changes in organic carbon could also be caused by a change in source. The 50% reduction in the mean organic carbon content in this fraction corresponds to the depth of the 1955-1964 horizon (48-59 cm). This time period has also been correlated to peak timber production in the basin (Hackett, 1999). Because a large amount of the organic carbon from this fraction is derived from discrete woody pieces it is logical to conclude that intense logging and sawmill activity would generate more discrete woody debris. Therefore, the apparent downcore reduction in weight %OC can also be explained by a lower input of wood debris before 1955-1964.

As noted above, clays were the focus of this study because they are typically associated with the bulk of sedimentary organic carbon buried on continental margins (Keil et al., 1994; Mayer, 1994a,b; Keil et al., 1997; Bock and Mayer, 2000). Analysis showed that the $\delta^{13}\text{C}_{\text{PDB}}$ values of the clay-sized particles were not affected by the change in sedimentation rate with means of $-24.1 \pm 0.3\text{‰}$ above 60 cm and $-23.8 \pm 0.2\text{‰}$ below 60 cm. The carbon loading of the clay particles, however, increases abruptly with the decrease in accumulation rate (Fig. 4.5). Loading values above 60 cm are approximately 70% of loading values below. This change in carbon loading was correlated to both a downcore decrease in surface area and increase in %OC (correlation coefficients = -0.78 and 0.73, respectively; Fig. 4.6).

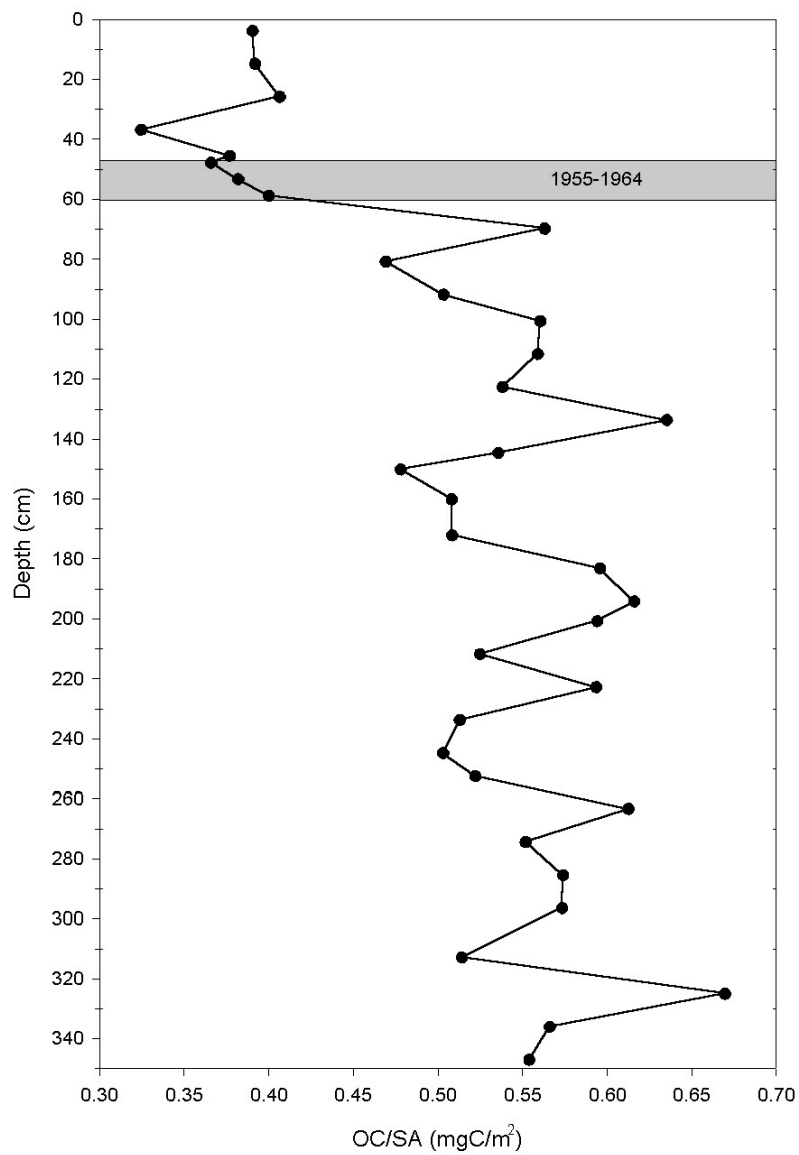


Figure 4.5. Organic carbon loading of the clay isolate from the K70 piston core. An abrupt 30% increase in mean OC loading is recorded below the 1955-1964 flood deposit.

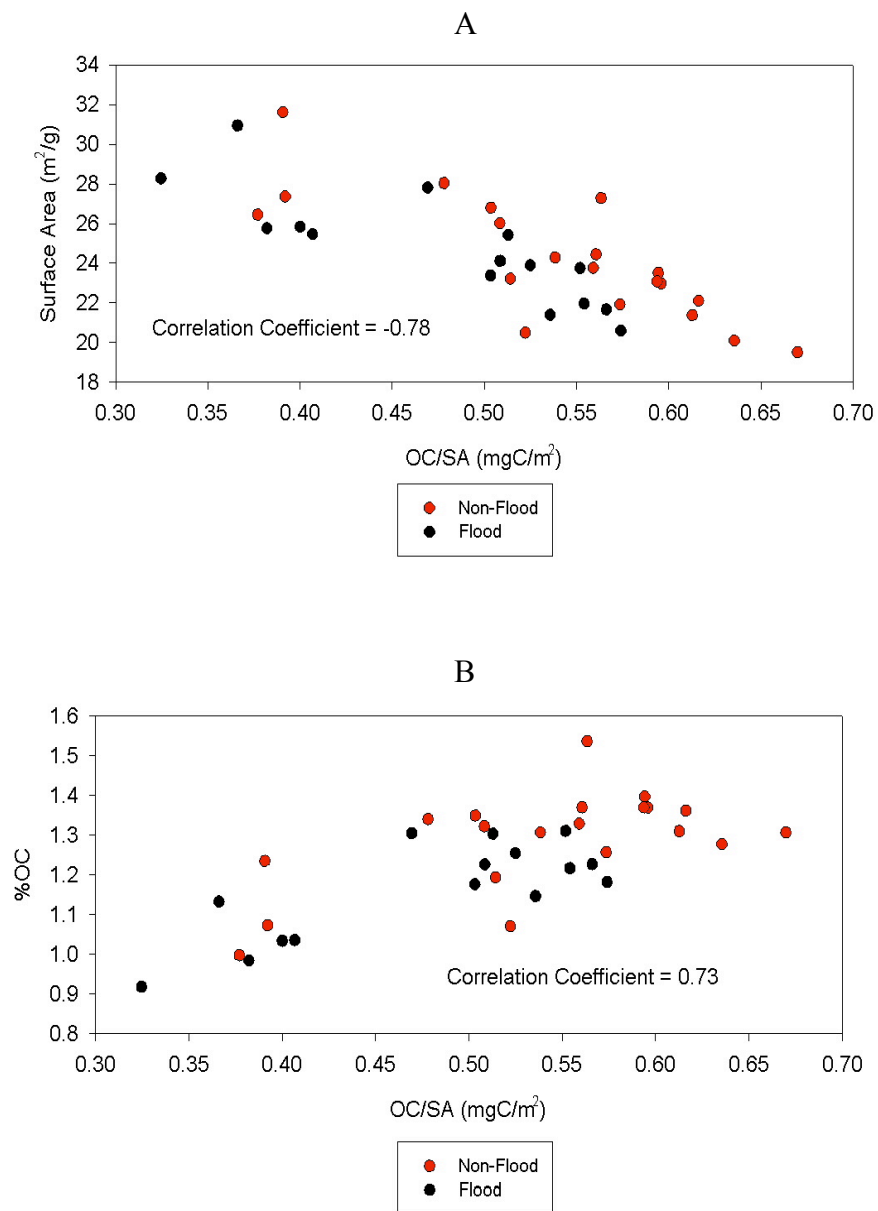


Figure 4.6. Correlations between the increase in OC/SA at 60 centimeters depth in the K70 piston core and change in clay surface area (A), and organic carbon content (B).

Analysis of the surface area of the clay fraction showed that there was a correlation between increasing depth and decreasing surface area ($r^2=0.59$; Fig. 3.11). There are two possible explanations for the decrease in clay surface area. First, because bulk grain size of the core increases below 60 cm, it is possible that the clay fraction itself might also be coarser below this depth, and thus have a lower surface area. Results from the grain size analysis of the clay isolate, however, showed no obvious coarsening down core (Fig. 3.5). Procedures for the high-resolution grain-size analysis of the clay fraction included sonication and exposure to hydrogen peroxide in order to break up aggregates of clay. These steps were not performed on clays analyzed for surface area, and thus the decreased surface area with depth may be attributed to more efficient aggregation from increased compaction downcore.

A second possible explanation for lower surface areas downcore is a change in the clay mineralogy. Results from the XRD study, however, indicated no significant change in mineralogy in the core. A constant mixture of chlorite, illite, smectite, quartz, and possibly vermiculite was found at all depths. These results are consistent with the regional geology and climate, as well as prior mineralogical studies in the region (Griggs and Hein, 1980; Karlin, 1980; Ransom et al., 1998). However, it should be noted that methods used in the examination of the clay mineralogy did not allow for a quantitative analysis, and while no large-scale change in mineralogy was detected with the XRD, it is possible that small changes in the concentrations of the different clay minerals were not detected in this study. Evidence for slight changes in the clay mineralogy

downcore has been documented on the Eel shelf (Holmes, in progress). Through the use of Fourier Transform Infrared Spectroscopy (FTIR), varying amounts of kaolinite have been detected in the shelf sediments. XRD investigations indicated no measurable amount of kaolinite, however, due to its highly ordered nature trace amounts of kaolinite can be detected with FTIR (Estep-Barnes, 1977). Since clay surface areas are highly variable from mineral to mineral (Evangelou, 1998) it is possible that such slight changes in mineralogy might provide a reason for the change in surface area down core.

Mean clay surface areas above and below 60 cm in the piston core differ by 3.4 m²/g. By assigning approximate surface areas to chlorite (150 m²/g) and smectite (200 m²/g), it was calculated that the downcore reduction in surface area could be attributed to decreases in chlorite by 2.5%, or smectite by 1.9% (Evangelou, 1998; Quirk and Murray, 1999). Gully erosion on the shaley *mélange*, grassland slopes dominates the recent source of sediment to the shelf (Kelsey, 1980). However, prior to the development of these gullies, landslides on the forested, sandstone slopes are believed to be responsible for most of the sediment delivered to the shelf (Kelsey, 1980). Such a change in sediment source could account for the alteration of clay content and ultimately explain the change in OC/SA at 60 cm.

The downcore increase in organic carbon loading on clay-sized particles in the K70 piston core also corresponds to a 20% increase in weight %OC. This increase in %OC likewise coincides with the decrease in sediment accumulation rate. Changes in sedimentation rates would result in changes in particle residence

times in different parts of the Eel basin, and in turn impact the amount of organic carbon associated with the mineral matrix. A study of surface Eel shelf sediments by Blair et al. (2003) found that three different fractions of carbon were bound to particles. The organic carbon in association with clays was classified as being derived from a marine, terrestrial, and ancient, mélange bedrock (kerogen) source. In addition, the study found that half of the organic carbon loaded to these clay particles was classified as being ancient carbon.

An observed decrease in accumulation rate in the shelf environment would correspond with decreased rates of denudation in the terrestrial environment. Slower removal of sediment from land would lengthen residence times in the regolith and thus prolong exposure time to terrestrial organic carbon sources. Likewise, exposure time in the benthic mixed zone on the shelf would also be prolonged due to the decreased burial rate associated with slower sedimentation. Assuming that particles being moved through the Eel watershed originated with only ancient sedimentary OC associated with them, it would be expected that sediments delivered to the shelf at reduced rates would have more recent terrestrial and marine OC associated with them due to their prolonged exposure to both types of OC sources.

Isotopic mass balance equations (Blair et al., 2003) were used to calculate the relative amounts of kerogen, marine, and terrestrial organic carbon associated with nine clay isolates from different depths in the K70 cores. The isotopic mass balance equations are:

$$\delta = f_k(\delta_k) + f_t(\delta_t) + f_m(\delta_m) \quad (1)$$

$$\delta_s = f_k(\delta_k) + f_t(\delta_t) + f_m(\delta_m) \quad (2)$$

$$1 = f_k + f_t + f_m \quad (3)$$

where δ_s , δ_k , δ_t , δ_m are the $\delta^{13}\text{C}$ values of the sample, and the kerogen, terrestrial and marine C end members. Likewise, δ_x and f_x represent the $\delta^{14}\text{C}$ and fraction for each of the above. The $\delta^{13}\text{C}$ end members for kerogen, marine and terrestrial C were determined to be -24.3‰, -21.0‰, and -26.5‰, respectively (Blair et al., 2003). Because the kerogen end member is ancient carbon, a $\delta^{14}\text{C}$ value of -1000 was assigned for the δ_k . When possible, the $\delta^{14}\text{C}$ of the wood fibers from the corresponding core depth was used to estimate the δ_t . Because wood fibers were not available for the box core samples, a modern $\delta^{14}\text{C}$ value of 100 was substituted, based on a regression from the Blair et al study (2003). The marine $\delta^{14}\text{C}$ was also set to 100 for modern samples, based on regression (Blair et al., 2003), but with increased depth down core this end member value was estimated by considering the average accumulation rate and the following equations derived from Stuiver and Polach (1977):

$$A_{(o,t)} = (\delta_{(o,t)}/1000 + 1) \cdot 0.95(0.306) \quad (4)$$

$$A_t = A_o e^{-\lambda t} \quad (5)$$

where A_t is the activity of ^{14}C at time t , A_o is the activity at $\delta_o = 0$, δ_t is the $^{14}\text{C}/^{12}\text{C}$ ratio at time t , λ is the decay rate for ^{14}C , and t is the age estimated from the accumulation rate.

Figures 4.7 and 4.8 show the results of these calculations for samples above and below the observed change in accumulation rate respectively. As with

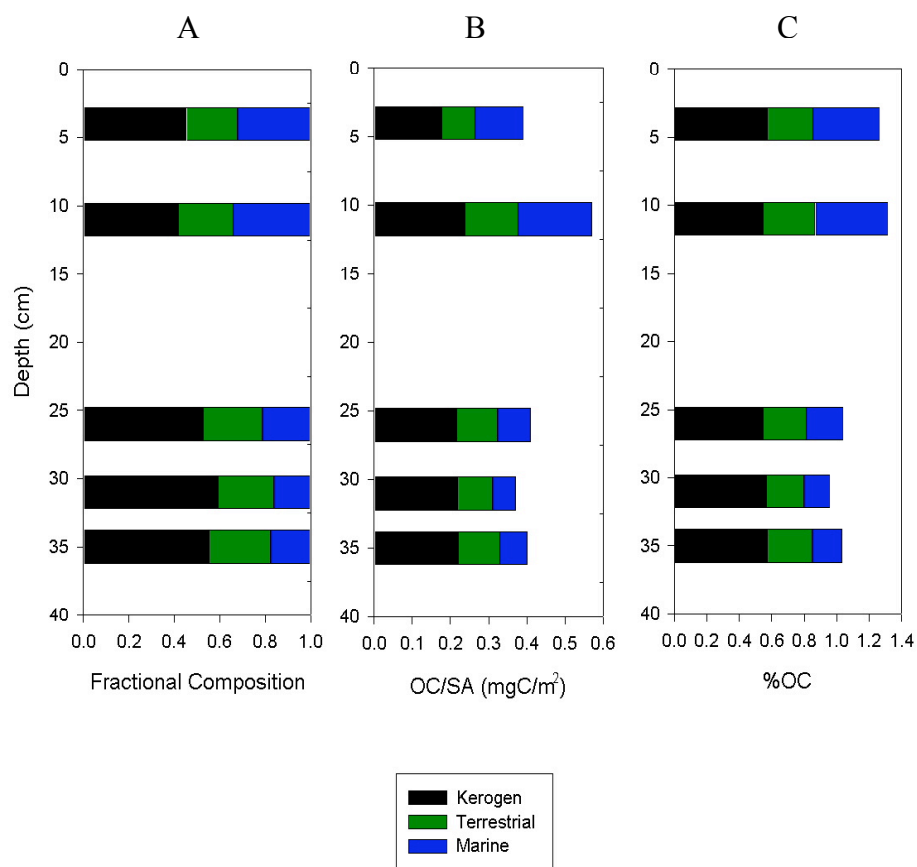


Figure 4.7. The kerogen, terrestrial, and marine components of total OC (A), total OC normalized to surface area (B), and total OC normalized to weight %OC (C) for shallow (<60 cm depth) samples. Approximately half of the total OC (40-60%) is from a kerogen source. The amount of kerogen OC loaded to the clay particles at these depths is approximately 0.2 mg C/m².

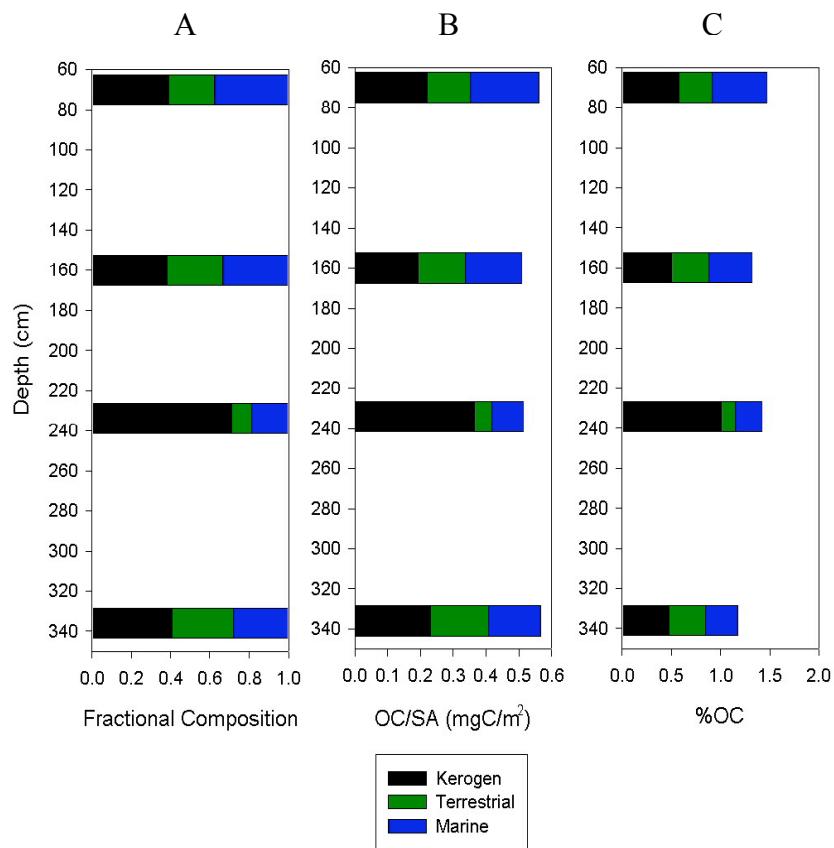


Figure 4.8. The kerogen, terrestrial, and marine components of total OC (A), total OC normalized to surface area (B), and total OC normalized to weight %OC (C) for samples below 60 cm depth. For 3 out of 4 samples, approximately half (40%) of the total OC is from a kerogen source. These samples also have a kerogen OC loading level of approximately 0.2 mg C/m². The sample from 234 cm depth is from a flood layer, and has a higher amount of kerogen OC associated with it (70% of the total OC).

the Blair et al. (2003) study, results of the isotopic mass balance for 8 of 9 samples in this investigation indicated that approximately half (40-60%) of the OC associated with clay particles was derived from a kerogen source. When kerogen OC/SA values were examined for these 8 samples a constant loading level equal to approximately 0.2 mg C/m^2 was observed. Therefore the increase in total OC/SA below the change in accumulation rate must be due to increases in either terrestrial OC or marine OC, or both. Figure 4.8 illustrates instances of both marine and terrestrial loading levels increasing below 60 cm depth, and thus indicates that the higher OC/SA values below 60 cm depth is due to more marine and terrestrial OC being preserved with the clay particles.

One of the four samples below 60 cm showed a decrease in marine and terrestrial OC/SA levels. The sample from 234 cm depth in the piston core had 70% of the OC loaded onto it coming from a kerogen source. This sample was found in association with a flood layer, which might offer some insight into why the composition of its OC differs from the other samples. Because of its association with a flood, these sediments would have been buried rapidly on the shelf, thus reducing exposure time to marine carbon, which could result in lower levels of marine carbon loaded to the particles. If the flood sediments from 234 cm depth were associated with a large flood event then the clays in this horizon may have been derived from a less weathered source rock, and therefore had much less exposure to contemporary terrestrial plants. Under these conditions one would expect to see what was found in the 234 cm sediment, that most of the sedimentary carbon came from the ancient kerogen source (Fig. 4.8).

5. Summary and Conclusions

Accumulation rates on the middle Eel shelf have not been constant over historic time. Based on ^{14}C -data from clay and wood fragments from the K70 piston core, accumulation rates over the last 50 years were estimated to be between 0.9-1.4 cm/yr, while a constant accumulation rate of 0.15 ± 0.02 cm/yr was calculated for the previous 1900 years. The change in shelf sedimentation also correlated with a downcore coarsening in sediment grain size and dated to a period between 1955-1964. Prior studies have cited higher flood frequency and water discharge of the Eel River over the last 50 years as the major cause for the changes in shelf sedimentation (Creamer, 1998; Sommerfield and Nittourer, 1999; Sommerfield et al., 2002). However, paleo-discharge records of the nearby Sacramento River indicated that current levels of wetness are not unique over the last 2000 years. Historical records indicate that industrial logging in the region reached its peak at a time that corresponds with changes in sedimentation rates, and old growth woody debris pieces were only found at depths below this change in sedimentation rate. Therefore recent higher accumulation rates on the shelf may be due in large part to deforestation that drastically altered land use in the Eel River water shed during the middle 20th century.

Examination of the organic carbon associated with Eel shelf sediments showed that the bulk of the OC is within the coarse ($>25\mu\text{m}$) fraction instead of the clay fraction ($<4\mu\text{m}$). The organic carbon in the coarse fraction is composed mostly of discrete woody pieces. Average %OC of this fraction decreases by approximately 50% below the accumulation rate change correlated to 1955-1964.

This decrease in woody organic carbon could be due to diagenesis, lower logging and saw mill activities, or a combination of both.

Unlike the coarse fraction, the organic carbon associated with the clay fraction ($<4\mu\text{m}$) shows a downcore increase attendant with the decreased accumulation rate. The average organic carbon loading (OC/SA) of clay particles above 60 cm is approximately 30% lower than the average loading level below. This change in loading reflects an approximate 20% downcore increase in average weight %OC from 1.05% to 1.3% at 60 cm, and a correlation between increasing depth and decreasing clay surface area. Isotopic mass balances of the organic carbon associated with the clay particles indicates that the higher weight %OC below 60 cm may be the result of more marine and terrestrial carbon being loaded to the sediments. Decreases in clay surface area with increasing depth may be the result of either a slight change in clay mineralogy associated with changing styles of mass wasting in the watershed, or the more complete aggregation of clay particles due to increased compaction with depth in the seabed.

References

- Aller, R.C., Blair, N.E., Xia, Q., and Rude, P.D., 1996, Remineralization rates, recycling, and storage of carbon in Amazon shelf sediments: *Continental Shelf Research*, v.16, p. 753-786.
- Beasley, T.M., Carpenter, R., and Jennings, C.D., 1982, Plutonium, ^{241}Am and ^{137}Cs ratios, inventories and vertical profiles in Washington and Oregon continental shelf sediments: *Geochimica et Cosmochimica Acta*, v.46, p. 1931-1946.
- Berner, R.A., 1982, Burial of organic carbon and pyrite sulfur in the modern ocean: its geochemical and environmental significance: *American Journal of Science*, v.282, p. 451-473.
- Berner, R.A., 1989, Biogeochemical cycles of carbon and sulfur and their effect on atmospheric oxygen over Phanerozoic time: *Palaeogeography, Palaeoclimatology, and Palaeoecology*, v.73, p. 97-122.
- Blair, N.E., Leithold, E.L., Ford, S.T., Peeler, K.A., Holmes, J.C., and Perkey, D.W., 2003, The persistence of memory: the fate of ancient sedimentary organic carbon in a modern sedimentary system: *Geochimica et Cosmochimica Acta*, v.67, p. 63-73.
- Blair, N.E., and Carter W.D., 1992, The carbon isotope geochemistry of acetate from a methanogenic marine sediment: *Geochimica et Cosmochimica Acta*, v.56, p. 1247-1258.

- Blake, M.C. Jr., Jayko, A.S., McLaughlin, R.J., and Underwood, M.B., 1988, Metamorphic and tectonic evolution of the Franciscan Complex, northern California. In: Ernst, W.G., ed. *Metamorphism and Crustal Evolution of the Western United States*. Prentice-Hall, Upper Saddle River, New Jersey. pp. 1036-1060.
- Blatt, H., Middleton, G., and Murray, R., 1980, *Origin of Sedimentary Rocks*. Prentice-Hall Inc., New Jersey, 782 p.
- Bock, M.J., and Mayer, L.M., 2000, Mesodensity organo-clay associations in a near-shore sediment: *Marine Geology*, v.163, p. 65-75.
- Brown, W.M., and Ritter, J.R., 1971, Sediment transport and turbidity in the Eel River basin, California: U.S. Geological Survey Water-Supply Paper 1986, 70 p.
- Brunauer, S., Emmett, P.H., and Teller, E., 1938, Adsorption of gases in multimolecular layers: *Journal of American Chemical Society*, v.30, p. 309-319.
- Burger, R.L., Fulthorpe, C.S., and Austin, J.A., 2001, Late Pleistocene channel inclusions in the southern Eel River basin, northern California: implications for tectonic versus eustatic influences on shelf sediment patterns: *Marine Geology*, v.177, p. 317-330.
- Clarke, S.H., 1992, Geology of the Eel River basin and adjacent region: implications for late Cenozoic tectonics of the southern Cascadia subduction zone and Mendocino Triple Junction: *The American Association of Petroleum Geologists Bulletin*, v.76, p. 199-224.

- Creamer, T.N., 1998, Sedimentology and flood-derived stratigraphy on the middle continental shelf off northern California. M.S. Thesis, NCSU, Raleigh, NC, 70 p.
- Dixon, J.B., and White, G.N., 1995, Soil mineralogy laboratory manual-Agronomy 626, Texas A&M University, published by the authors.
- Erickson, J., 1986, Marine Geology. Facts on File Inc., New York, 243 p.
- Estep-Barnes, P., 1977, Infrared spectroscopy, chapter 11. In: Zussman, J., ed. Physical Methods in Determinative Mineralogy, 2nd Edition. Academic Press, New York.
- Evangelou, V.P., 1998, Environmental Soil and Water Chemistry Principles and Applications. John Wiley & Sons, New York, 564 p.
- Foster, G., and Carter, L., 1997, Mud sedimentation on the continental shelf at an accretionary margin – Poverty Bay, New Zealand: New Zealand Journal of Geology and Geophysics, v.40, p. 157-173.
- Fry, B., and Sherr E.B., 1984, $\delta^{13}\text{C}$ measurements as indicators of carbon flow in marine and freshwater ecosystems: Contributions in Marine Science, v.27, p. 13-47.
- Gavin, D.G., 2001, Estimation of inbuilt age in radiocarbon ages of soil charcoal for fire history studies: Radiocarbon, v.43, p. 27-44.
- Geyer, W.R., Hill, P., Milligan, T., and Traykovski, P., 2000, The structure of the Eel River plume during floods: Continental Shelf Research, v.20, p. 2067-2093.
- Goff, J.R., 1997, A chronology of natural and anthropogenic influences on coastal sedimentation, New Zealand: Marine Geology, v.138, p. 105-117.

- Goni, M.A., Ruttenger, K.C., and Eglinton, T.I., 1998, A reassessment of the sources and importance of land-derived organic matter in surface sediments from the Gulf of Mexico: *Geochimica et Cosmochimica Acta*, v.62, p. 3055-3075.
- Griggs, G.B., and Hein, J.R., 1980, Sources, dispersal, and clay mineral composition of fine-grained sediment off central and northern California: *Journal of Geology*, v.88, p. 541-566.
- Hackett, S.C., 1999, The Humboldt County economy: where have we been and where are we going, Humboldt State University, 2 p. (www.humboldt.edu/~economic/humcoecon.html).
- Hartnett, H.E., Keil, R.G., Hedges, J.I., and Devol, A.H., 1998, Influence of oxygen exposure time on organic carbon preservation in continental margin sediments: *Nature*, v.391, p. 572-574.
- Hayes, J.M., DesMarais, D.J., Peterson, D.W., Schoeller, D.A., and Taylor, S.P., 1977, High precision stable isotope ratios from microgram samples: *Advances in Mass Spectrometry*, v.7, p. 475-480.
- Hedges, J.I., Clark, W.A., and Cowie, G.L., 1988, Organic matter sources to the water column and surficial sediments of a marine bay: *Limnology and Oceanography*, v.33, p. 1116-1136.
- Hedges, J.I., and Keil, R.G., 1995, Sedimentary organic matter preservation: An assessment and speculative synthesis: *Marine Chemistry*, v.49, p. 81-115.

- Helley, E.J., and LaMarche, V.C., 1973, Historic flood information for northern California streams from geological and botanical evidence, U. S. Geological Survey Professional Paper 485-E, 16 p.
- Hicks, M.D., Gomez, B., Trustrum, N.A., 2000, Erosion thresholds and suspended sediment yields, Waipaoa River basin, New Zealand: *Water Resources Research*, v.36, p. 1129-1142.
- Hilfinger, M.F., Mullins, H.T., Burnett, A., and Kirby, M.E., 2001, A 2500 year sediment record from Fayetteville Green Lake, New York: evidence for anthropogenic impacts and historic isotope shift: *Journal of Paleolimnology*, v.26, p. 293-305.
- Karlin, R., 1980, Sediment sources and clay mineral distributions off the Oregon coast: *Journal of Sedimentary Petrology*, v.50, p. 543-560.
- Keil, R.G., Mayer, L.M., Quay, P.D., Richey, J.E., and Hedges, J.I., 1997, Loss of organic matter from riverine particles in deltas: *Geochimica et Cosmochimica Acta*, v.61, p. 1507-1511.
- Keil, R.G., Tsamakis, E., Bor Fuh, C., Giddings, J.C., and Hedges, J.I., 1994, Mineralogical and textural controls on the organic composition of coastal marine sediments: hydrodynamic separation using SPLITT fractionation: *Geochimica et Cosmochimica Acta*, v.58, p. 879-893.
- Keith, M.L., and Weber, J.N., 1964, Carbon and oxygen isotopic composition of selected limestones and fossils: *Geochimica et Cosmochimica Acta*, v.28, p. 1787-1816.

- Kelsey, H.M., 1980, A sediment budget and analysis of geomorphic process in the Van Duzen River basin, north central California, 1941-1975: summary: Geological Society of America Bulletin Part I, v.91, p. 190-195.
- Leithold, E.L., 1989, Depositional processes on an ancient and modern muddy shelf, northern California: *Sedimentology*, v.36, p. 179-202.
- Leithold, E.L., and Blair, N.E., 2001, Watershed control on the carbon loading of marine sedimentary particles: *Geochimica et Cosmochimica Acta*, v.65, p. 2231-2240.
- Leithold, E.L., and Hope, R.S., 1999, Deposition and modification of a flood layer on the northern California shelf: lessons from and about the fate of terrestrial particulate organic carbon: *Marine Geology*, v.154, p. 183-195.
- Mayer, L.M., 1994a, Surface area control of organic carbon accumulation in continental shelf sediments: *Geochimica et Cosmochimica Acta*, v.58, p. 1271-1284.
- Mayer, L.M., 1994b, Relationships between mineral surfaces and organic carbon concentrations in soils and sediments: *Chemical Geology*, v.114, p. 347-363.
- Meko, D.M., Therrell, M.D., Baisan, C.H., and Hughes, M.K., 2001a, Sacramento River flow reconstruction to A.D. 869 from tree rings: *Journal of the American Water Resources Association*, v.37, p. 1029-1039.
- Meko, D.M., Therrell, M.D., Baisan, C.H., and Hughes, M.K., 2001b, Sacramento River annual flow reconstruction. International Tree-Ring Data Bank. IGBP Pages/World Data Center for Paleoclimatology, series #2001-081. NOAA/NGDC Paleoclimatology Program, Boulder CO.

- Milliman, J.D., 1997, Fluvial sediment discharge to the sea and the importance of regional tectonics. In: William F. Ruddiman (ed.), *Tectonic Uplift and Climate Change*. Plenum Press, New York, p. 239-257.
- Milliman, J.D., and Syvitski, P.M., 1992, Geomorphic/tectonic control of sediment discharge to the ocean: the importance of small mountainous rivers: *Journal of Geology*, v.100, p. 525-544.
- Moore, D.M., and Reynolds, R.C., 1989, *X-Ray Diffraction and the Identification and Analysis of Clay Minerals*. Oxford University Press, New York, 332 p.
- Olsson, I.U., 1970, The use of oxalic acid as a standard. In *Radiocarbon Variations and Absolute Chronology*, Nobel Symposium, 12th Proc. Wiley & Sons, New York, 17 p.
- Orange, D.L., 1999, Tectonics, sedimentation and erosion in northern California: submarine geomorphology and sediment preservation potential as a result of three competing processes: *Marine Geology*, v.154, p. 369-382.
- Page, M.J., and Trustrum, N.A., 1997, A late Holocene lake sediment record of the erosion response to land use change in a steep-land catchment, New Zealand: *Zeitschrift für Geomorphologie N.F.*, v.41, p. 369-392.
- Page, M.J., Trustrum, N.A., and Gomez, B., 2000, Implications of a century of anthropogenic erosion for future land use in the Gisborne-East coast region of New Zealand: *New Zealand Geographer*, v.56, p. 9-20.
- Quirk, J.P., and Murray, R.S., 1999, Appraisal of the ethylene glycol monoethyl ether method for measuring hydratable surface area of clays and soils: *Soil Science Society of America Journal*, v.63, p. 839-849.

- Ransom, B., Dongseom, K., Kastner, M., and Wainwright, S., 1998, Organic matter preservation on continental slopes: importance of mineralogy and surface area: *Geochimica et Cosmochimica Acta*, v.62, p. 1329-1345.
- Rao, P.V., 1998, *Statistical Research Methods in the Life Sciences*. Brooks/Cole Publishing Co., Pacific Grove, California, 889 p.
- Rooney, J.J., and Smith, S.V., 1999, Watershed landuse and bay sedimentation: *Journal of Coastal Research*, v.15, p. 475-485.
- Seibold, E., Berger, W.H., 1996, *The Sea Floor: an Introduction to Marine Geology*. Springer, New York, 356 p.
- Sollins, P., Cline, S.P., Verhoeven, T., Sachs, D., and Spycher, G., 1987, Patterns of log decay in old-growth Douglas-fir forests: *Canadian Journal of Forest Research*, v.17, p. 1585-1595.
- Sommerfield, C.K., 1997, *Modern sedimentation and diagenetic processes on the Eel River shelf and slope, northern California continental margin*. Ph.D. Dissertation, State University of New York-Stony Brook, 281 p.
- Sommerfield, C.K., Aller, R.C., and Nittrouer, C.A., 2001, Sedimentary carbon, sulfur, and iron relationships in modern and ancient diagenetic environments of the Eel River basin: *Journal of Sedimentary Research*, v.71, p. 335-345.
- Sommerfield, C.K., Drake, D.E., and Wheatcroft, R.A., 2002, Shelf record of climate changes in flood magnitude and frequency, north-coastal California: *Geology*, v.30, p. 395-398.

- Sommerfield, C.K., and Nittrouer, C.A., 1999, Modern accumulation rates and sediment budget for the Eel shelf: a flood-dominated depositional environment: *Marine Geology*, v.154, p. 227-241.
- Stone, J.N., MacKinnon, A., Parminter, J.V., and Lertzman, K.P., 1998, Coarse woody debris decomposition documented over 65 years on southern Vancouver Island: *Canadian Journal of Forest Research*, v.28, p. 788-793.
- Strub, P.T., and Corinne, J., 2002, Altimeter-derived surface circulation in the large-scale NE Pacific Gyres, Pt.1. seasonal variability: *Progress in Oceanography*, v.53, p. 163-183.
- Stuiver, M., and Polach, H.A., 1977, Reporting of ^{14}C data: *Radiocarbon*, v.19, p. 355-363.
- Syvitski, J.P., and Morehead, M.D., 1999, Estimating river-sediment discharge to the ocean: application to the Eel margin, northern California: *Marine Geology*, v.154, p. 13-28.
- U.S. Environmental Protection Agency, 1999a, Van Duzen and Yager Creek total maximum daily load for sediment: San Francisco, California, Environmental Protection Agency Region IX Water Division, 57 p. (www.epa.gov/region09/water/tmdl/final.html).
- U.S. Environmental Protection Agency, 1999b, South Fork Eel River total maximum daily loads for sediment and temperature: San Francisco, California, Environmental Protection Agency Region IX Water Division, 62 p. (www.epa.gov/region09/water/tmdl/final.html).

- VanGeen, A., Valette-Silver, N.J., Luoma, S.N., Fuller, C.C., Baskaran, M., Tera, F., and Klein, J., 1999, Constraints on the sedimentation history of San Francisco Bay from ^{14}C and ^{10}Be : *Marine Chemistry*, v.64, p. 29-38.
- Walker, G.F., 1957, On the differentiation of vermiculites and smectites in clays: *Clay Mineralogy Bulletin*, v.3, 154-163.
- Wheatcroft, R.A., and Borgeld, J.C., 2000, Oceanic flood deposits on the northern California shelf: large-scale distribution and small-scale physical properties: *Continental Shelf Research*, v.20, p. 2163-2190.

Appendices

Appendix A: Grain-size Data
Grain-size data for K70 piston core

Section	Depth (cm)	%>25 μm	%4–25 μm	%<4 μm
7 (3-4)	4	38.54	47.36	14.11
7 (13-14)	15	47.84	39.14	13.03
7 (23-24)	26	23.53	60.94	15.53
7 (28-29)	31	54.06	36.56	9.37
7 (33-34)	37	34.05	37.01	28.94
7 (37-38)	41	61.05	29.06	9.89
7 (41-42)	46	49.97	41.15	8.88
6 (0-1.5)	48	35.30	42.67	22.04
6 (5-6)	53	30.31	42.68	27.01
6 (10-11)	59	22.80	50.16	27.04
6 (20-21)	70	63.92	25.81	10.28
6 (30-31)	81	52.54	34.70	12.75
6 (40-41)	92	63.26	25.35	11.39
5 (1-2)	101	77.20	13.37	9.43
5 (11-12)	112	68.30	19.00	12.70
5 (21-22)	123	71.42	17.86	10.73
5 (31-32)	134	75.45	14.74	9.81
5 (41-42)	145	42.32	41.63	16.05
4 (1-2)	150	72.41	17.06	10.53
4 (11-12)	160	76.68	13.91	9.41
4 (18-19)	169	61.45	27.91	10.63
4 (21-22)	172	61.08	24.43	14.49
4 (26-27)	178	53.27	32.12	14.61
4 (31-32)	183	76.87	13.35	9.78
4 (41-42)	194	75.99	14.78	9.23
3 (1-2)	201	70.54	21.28	8.18
3 (3-4)	203	69.22	21.42	9.36
3 (11-12)	212	57.39	31.63	10.98
3 (21-22)	223	76.94	16.08	6.98
3 (31-32)	234	62.29	26.48	11.23
3 (41-42)	245	58.81	29.79	11.40
3 (44-45)	248	56.30	31.65	12.06
2 (1-2)	252	70.60	17.94	11.47
2 (11-12)	263	64.82	26.23	8.95
2 (21-22)	274	59.98	30.76	9.26
2 (31-32)	285	56.99	30.35	12.66
2 (41-42)	296	68.88	21.25	9.87
2 (43-44)	299	67.28	23.95	8.77
1 (1-2)	303	69.58	22.31	8.11
1 (2-3)	304	68.79	23.62	7.60

Grain-size data for K70 piston core (continued)

Section	Depth (cm)	%>25 μm	%4–25 μm	%<4 μm
1 (10-11)	313	68.72	18.85	12.43
1 (21-22)	325	79.68	14.49	5.83
1 (27-28)	334	74.26	17.39	8.36
1 (31-32)	336	60.61	29.89	9.50
1 (41-42)	347	60.69	27.40	11.91

Grain-size data for K70 box core

Section	Depth (cm)	%>25 μm	%4–25 μm	%<4 μm
1 (1-2)	2	10.59	38.95	50.46
1 (4-5)	6	53.86	29.60	16.54
1 (5-6)	7	35.49	45.61	18.89
1 (6-7)	8	62.24	22.77	14.99
1 (7-8)	9	45.69	33.38	20.93
1 (8-9)	11	59.15	27.85	12.99
1 (10-11)	13	74.57	17.90	7.53
1 (12-13)	16	53.88	30.13	16.00
1 (14-15)	18	45.76	30.65	23.59
1 (16-17)	21	33.03	49.53	17.44
1 (18-19)	23	55.70	27.92	16.38
1 (20-21)	26	31.78	45.29	22.93
1 (22-23)	28	25.24	53.53	21.23
1 (24-25)	31	21.08	71.03	7.89
1 (26-27)	34	40.09	46.58	13.33
1 (27-28)	35	14.45	56.69	28.86
1 (28-29)	36	26.87	45.38	27.75
1 (29-30)	37	15.49	58.60	25.92
1 (30-31)	39	15.20	61.67	23.13
1 (32-33)	41	59.08	29.52	11.40
1 (34-35)	44	59.81	27.88	12.31
1 (36-36.5)	46	22.79	43.68	33.53

Appendix B: Organic Data

Clay organic data for K70 piston core

Section	Depth (cm)	$\delta^{13}\text{C}$	Weight %OC	OC/SA (mgC/m ²)
7 (3-4)	4	-23.65	1.24	0.39
7 (13-14)	15	-24.07	1.07	0.39
7 (23-24)	26	-24.18	1.04	0.41
7 (33-34)	37	-24.53	0.92	0.32
7 (41-42)	46	-23.90	1.00	0.38
6 (0-1.5)	48	-23.66	1.13	0.37
6 (5-6)	53	-24.14	0.98	0.38
6 (10-11)	59	-24.50	1.03	0.40
6 (20-21)	70	-23.52	1.54	0.56
6 (30-31)	81	-23.78	1.31	0.47
6 (40-41)	92	-23.89	1.35	0.50
5 (1-2)	101	-23.51	1.37	0.56
5 (11-12)	112	-23.47	1.33	0.56
5 (21-22)	123	-23.54	1.31	0.54
5 (31-32)	134	-23.75	1.28	0.64
5 (41-42)	145	-23.96	1.15	0.54
4 (1-2)	150	-23.66	1.34	0.48
4 (11-12)	160	-23.85	1.32	0.51
4 (21-22)	172	-24.09	1.23	0.51
4 (31-32)	183	-23.65	1.37	0.60
4 (41-42)	194	-23.83	1.36	0.62
3 (1-2)	201	-23.81	1.40	0.59
3 (11-12)	212	-23.83	1.25	0.52
3 (21-22)	223	-23.57	1.37	0.59
3 (31-32)	234	-23.69	1.30	0.51
3 (41-42)	245	-23.99	1.18	0.50
2 (1-2)	252	-24.22	1.07	0.52
2 (11-12)	263	-23.97	1.31	0.61
2 (21-22)	274	-23.77	1.31	0.55
2 (31-32)	285	-24.08	1.18	0.57
2 (41-42)	296	-23.98	1.26	0.57
2 (43-44)	299	-23.89	1.30	
1 (2-3)	304	-23.77	1.41	
1 (10-11)	313	-23.86	1.19	0.51
1 (21-22)	325	-23.76	1.31	0.67
1 (27-28)	334	-24.00	1.33	
1 (31-32)	336	-23.89	1.23	0.57
1 (41-42)	347	-23.98	1.22	0.55

>25 μm organic data for K70 piston core

Section	Depth (cm)	$\delta^{13}\text{C}$	Weight %OC	Atomic C/N
7(3-4)	4	-26.06	1.73	29.81
7(41-42)	46	-25.57	1.17	34.81
6(20-21)	70	-25.34	0.85	26.46
4(11-12)	160	-25.20	0.68	22.48
3(31-32)	234	-25.29	0.62	24.73
1(31-32)	336	-25.25	0.67	24.78

<25 μm organic data for K70 piston core

Section	Depth (cm)	$\delta^{13}\text{C}$	Weight %OC	Atomic C/N
7(3-4)	4	-24.20	0.85	12.31
7(41-42)	46	-24.42	0.50	13.61
6(20-21)	70	-24.20	0.88	12.64
4(11-12)	160	-24.28	0.93	12.88
3(31-32)	234	-24.45	0.85	12.99
1(31-32)	336	-24.51	0.86	12.16

Bulk organic data for K70 piston core

Section	Depth (cm)	$\delta^{13}\text{C}$	Weight %OC	Atomic C/N
7(3-4)	4	-25.17	1.29	21.19
7(41-42)	46	-25.30	0.68	21.06
6(20-21)	70	-24.69	0.96	21.74
4(11-12)	160	-24.98	0.95	21.98
3(31-32)	234	-24.92	0.84	18.29
1(31-32)	336	-24.84	0.90	18.49

Clay organic data for K70 box core

Section	Depth (cm)	$\delta^{13}\text{C}$	Weight %OC	OC/SA (mgC/m^2)
1 (1-2)	2	-24.57	0.92	0.35
1 (2-3)	3	-23.98		
1 (5-6)	7	-23.90	1.18	0.38
1 (6-7)	8	-24.19	1.18	0.48
1 (12-13)	16	-23.82	1.21	0.45
1 (16-17)	21	-23.96	1.16	0.43
1 (18-19)	23	-23.93	1.14	0.43
1 (28-29)	36	-24.34	0.95	0.37
1 (30-31)	39	-24.50	1.11	0.46
1 (34-35)	44	-23.62	1.21	0.41

Appendix C: ^{14}C Data

^{14}C results for clays from K70 piston core

Sample	Depth (cm)	$\Delta^{14}\text{C}\%$	Age (years)
7 (3-4)	4	-402.7	4090
6 (20-21)	70	-410.8	4200
4 (11-12)	160	-437.7	4570
3 (31-32)	234	-753.8	11200
1 (31-32)	336	-527.2	5970

^{14}C results for wood from K70 piston core

Sample	Depth (cm)	$\Delta^{14}\text{C}\%$	Age (years)
7 (3-4)	4	80	-636
7 (41-42)	46	90.2	-713
6 (20-21)	70	-60.4	450
4 (11-12)	160	-108.6	875
3 (31-32)	234	-179.8	1540
1 (31-32)	336	-210.3	1850

^{14}C results for clay from K70 box core

Sample	Depth (cm)	$\Delta^{14}\text{C}\%$	Age (years)
1 (8-9)	11	-360.2	-
1 (20-21)	26	-480.1	-
1 (24-25)	31	-552.5	-
1 (27-28)	35	-509	-